Optimum Design of High-Speed Prop-Rotors

Final Report

Grant Number: NAG2-771

Principal Investigator - Aditi Chattopadhyay

Graduate Research Associate - Thomas Robert McCarthy

Department of Mechanical and Aerospace Engineering
Arizona State University
Tempe, Arizona

Abstract

An integrated multidisciplinary optimization procedure is developed for application to rotary wing aircraft design. The necessary disciplines such as dynamics, aerodynamics, aeroelasticity, and structures are coupled within a closed-loop optimization process. The procedure developed is applied to address two different problems. The first problem considers the optimization of a helicopter rotor blade and the second problem addresses the optimum design of a high-speed tilting proprotor. In the helicopter blade problem, the objective is to reduce the critical vibratory shear forces and moments at the blade root, without degrading rotor aerodynamic performance and aeroelastic stability. In the case of the high-speed proprotor, the goal is to maximize the propulsive efficiency in high-speed cruise without deteriorating the aeroelastic stability in cruise and the aerodynamic performance in hover. The problems studied involve multiple design objectives; therefore, the optimization problems are formulated using multiobjective design procedures. A comprehensive helicopter analysis code is used for the rotary wing aerodynamic, dynamic and aeroelastic stability analyses and an algorithm developed specifically for these purposes is used for the structural analysis. A nonlinear programming technique coupled with an approximate analysis procedure is used to perform the optimization. The optimum blade designs obtained in each case are compared to corresponding reference designs.

Table of Contents

Page

List of Tables viii

List of Figures ix

Nomenclature xi

I. Introduction 1

Helicopter Design Considerations 1

Helicopter Rotor Blade Optimization 3

Sequential Optimization 3

Multidisciplinary Optimization 4

High-Speed Rotorcraft Design Considerations 5

High-Speed Rotorcraft Optimization 6

Multiple Design Objectives 7

II. Objectives 9

III. Multiobjective Optimization 10

Modified Global Criteria Approach 10

Minimum Sum Beta (Min $\Sigma\beta$) Approach 11

Kreisselmeier-Steinhauser (K-S) Function Approach 12

Problem Statement 13

Blade model 14

Optimization 17

Analysis 19

Dynamic, Aerodynamic and Aeroelastic Analyses 19

Structural Analysis 19

Optimization Implementation 20

Page

Results and Discussions....21

Conclusions....30

IV. Integrated Helicopter Rotor Blade Optimization....33

Problem Definition....33

Blade Model....34

Optimization....38

Analysis....40

Dynamic, Aerodynamic and Aeroelastic Analyses....40

Structural Analysis....41

Optimization Implementation....41

Results and Discussions....41

Conclusions....53

V. Integrated High-Speed Proprotor Optimization....55

Problem Definition....55

Blade Model....55

Optimization....57

Analysis....58

Dynamic, Aerodynamic and Aeroelastic Analyses....58

Structural Analysis....59

Optimization Implementation....59

Results and Discussions....61

Conclusions....76

VI. References....78

List of Tables

Table		Page
1	Summary of Multiobjective Optimization Constraints	23
2	Summary of Multiobjective Design Variables	23
3	Summary of Integrated Helicopter Rotor Blade Optimization Results	44
4	Summary of Integrated Helicopter Rotor Blade Optimization Design Variables	45
5	Summary of Integrated High-Speed Proprotor Optimization Results	63
6	Summary of Integrated High-Speed Proprotor Optimization Design Variables	65

List of Figures

Figure		Page
1	Simplified rotor blade model with linear taper	14
2	Centrifugal stress distribution	24
3	Lead-lag bending stiffness distribution	25
4	Nonstructural weight distribution	26
5	Comparison of individual objective functions	27
6	4/rev vertical shear iteration history	28
7	3/rev inplane shear iteration history	29
8	Objective function iteration history	30
9	Double-celled box beam configuration	33
10	Variation of tip shape with tip shape parameter, p	35
11	Variation of tip shape with tip shape parameter, α	36
12	Variation of blade twist with changes in tip shape parameter, δ	37
13	Comparisons of normalized vibratory loads and total power	46
14	Torsional bending stiffness distribution	47
15	Blade nonstructural weight distributions	48
16	Chord distribution	49
17	Blade center of gravity offset distribution	50
18	4/rev vertical shear iteration history	51
19	4/rev lagging moment iteration history	52
20	Objective function convergence history	53
21	Swept blade planform	57
22	Comparison of individual objective functions	64
23	Chord distribution	66

Figure Page

24 Flapwise bending stiffness distribution....67

25 Lead-lag bending stiffness distribution....68

26 Torsional bending stiffness distribution....69

27 Nonstructural weight distribution....70

28 Twist distribution....71

29 Sweep distribution....73

30 Lifting line distribution....74

31 Individual objective function iteration history....75

32 Objective function iteration history....76

Nomenclature

b_m	base of the m^{th} box beam member, ft
c	chord, ft
c_o - c_3	chord distribution parameters
f_i	natural frequency of the ith mode, per rev (/rev)
f_r	3/rev radial shear, lb
f_x	3/rev inplane shear, lb
f_z	4/rev vertical shear, lb
g_1, g_2, g_3	vector of constraint functions
$\hat{g}$	approximated constraint vector
h_m	height of the m^{th} box beam member, ft
k	principle radius of gyration, ft^2
m_c	3/rev torsional moment, lb-ft
m_x	3/rev flapping moment, lb-ft
m_z	4/rev lagging moment, lb-ft
p	chord distribution shape parameter
p_n	two point approximation exponent for the n^{th} design variable
t_m	box beam wall thickness of the m^{th} member, ft
w_{t_j}	leading edge nonstructural weight at the j^{th} node, lb/ft
w_{c_j}	central nonstructural weight at the j^{th} node, lb/ft
w_{sk_j}	blade skin weight at the j^{th} node, lb/ft
w_{hc_j}	honeycomb filler weight at the j^{th} node, lb/ft
x_e	nondimensional center of gravity offset forward of shear center
x, y, z	reference axes
$\bar{y}$	nondimensional radial location
$\hat{y}_j$	distance from the blade root to the center of the j^{th} segment, ft
A_j	average area of the j^{th} segment, ft^2
AI	autorotational inertia, $lb\text{-}ft^2$
C_T	thrust coefficient
C_p	power coefficient
EI_{xx}, EI_{zz}	bending stiffnesses, $lb\text{-}ft^2$
F_k	k^{th} objective function
F_{ko}	values of the objective function F_k at the beginning of an iteration
$\tilde{F}_1, \tilde{F}_2, \tilde{F}_3$	multiobjective formulation of the individual objective functions, F_k

$\bar{F}_k$	prescribed target of the objective function F_k
$\hat{F}_k$	approximated value of the objective function F_k
FOM	hover figure of merit
GJ	torsional stiffness, lb-ft^2
L_j	length of the j^{th} segment, ft
M	total number of constraints and objective functions
NCON	number of constraints
NDV	number of design variables
NOBJ	number of objective functions
NSEG	number of blade segments
NMEM	number of box beam structural members
R	blade radius, ft
T	thrust, lb
W_{ns_i}	nonstructural weight of the j^{th} segment, lb
W_{s_i}	structural weight of the j^{th} segment, lb
W_j	total weight of the j^{th} segment, lb
W	total blade weight, lb
α	chord distribution shape parameter
α_k	k^{th} aeroelastic stability root
β_1, β_2	pseudo design variables
$\varepsilon_1, \varepsilon_2$	lifting line curvature parameters
δ	twist shape parameter
λ_k	k^{th} eigenvalue of the Floquet transition matrix
$\tilde{\lambda}$	inverse taper ratio
μ	advance ratio
Φ	design variable vector
ϕ_i	i^{th} design variable
ρ	K-S function multiplier
θ	blade twist, degrees
θ_o - θ_3	blade twist distribution parameters
σ	area solidity
σ_i	stress in i^{th} segment, lb/ft^2
σ_{cent}	centrifugal stress, lb/ft^2
σ_{vib}	vibratory stress, lb/ft^2

τ	twist ratio
υ_k	minimum allowable aeroelastic damping for the k^{th} mode
ζ	prescribed bounds for blade distribution parameters
Ω	rotor angular velocity, revolutions per minute (RPM)
ω	rotor angular velocity, rad/sec

Subscripts

max	maximum value
r	value at the blade root
ref	reference blade value
t	value at the blade tip
L	lower bound
U	upper bound

I. Introduction

Design optimization methodologies have recently emerged as a practical tool in the design of aerospace vehicles[1] and an extensive amount of research has been conducted in bringing the state of the art in optimization techniques to a very high level[2,3]. Although these techniques have received widespread attention in the fixed-wing industry, they are less well-known in rotary wing applications. Previously, rotary wing design procedures relied heavily on the designer's experience as well as trial and error methods. However, with the improved understanding of rotorcraft analysis techniques, the availability of sophisticated computing resources and the existence of efficient optimization algorithms, it is now possible to use design optimization at both the preliminary and redesign stages of the development of rotary wing aircraft. In the following sections, brief descriptions of the design considerations in helicopter and high-speed proprotor aircraft along with optimization efforts in these fields are presented.

Helicopter Design Considerations

The conventional rotor blade design process consists of first designing the blade to satisfy certain aerodynamic requirements. This is followed by structural modeling and blade tuning based on dynamic analysis. The aerodynamic design process alone, consists of selection of variables such as blade planform, airfoils and twist. The process is further complicated by the often conflicting design requirements. For example, as indicated by Magee et al.[4] the "best" twist for hover produces negative angle of attack on inboard airfoil sections in forward flight conditions, whereas the "best" twist in forward flight causes the blade to stall inboard in hover. Similar conflicts also occur in the choice of the chord distributions. These trade-offs necessitate the use of parametric studies to be completed prior to the selection of such parameters. This process is tedious and computationally expensive and can be avoided by implementing appropriate design optimization strategies.

Vibration has long been a major source of problems in helicopters and its alleviation plays an important role in the rotor blade design process. The potential sources for helicopter vibrations are rotors, engines and gear boxes and each produces loads over a wide range of frequencies. These vibrations can be categorized as low and high frequency vibrations. The high frequency vibrations are mainly acoustic and are not responsible for mechanical failures, except for some isolated cases of structural resonance. The low frequency vibrations are the cause of all fatigue-related failures and are therefore of importance not only to the rotor system but also to the airframe. For a helicopter in forward flight, the nonuniform flow passing through the rotor causes oscillating airloads on the rotor blades which are translated into vibratory shear forces and bending moments at the hub. In the rotor system itself, loads are present at all harmonics of rotor speed, but the symmetry of the rotor system ensures that significant loads are transmitted to the airframe only at multiples of the rotor passing frequency (i.e. inΩ, where i is an integer, n represents the number of blades and Ω is the rotor RPM.). The biggest component of the airframe vibratory forces occur at the fundamental blade passing frequency (nΩ). This involves consideration of the rotor responses to airloads at n$\pm$1 harmonics as well[5]. Because a rotor producing low hub loads will produce low vibration throughout the airframe, vibration alleviation plays a major role in the rotor blade design. As indicated in a survey by Reichert[6], it is necessary to consider vibration reduction throughout the development phase of the helicopter. The survey also outlines the various existing methods of reducing helicopter vibration such as the use of special absorbers at the rotor blades or the hub. More innovative vibration techniques, such as active higher harmonic control and vibrational isolation of the fuselage from the rotor/transmission assembly based on antiresonance, are also discussed. The use of structural optimization in the early stages of the design process is suggested as a mechanism for reducing the "main-in-the-loop" type of iterations.

Helicopter Rotor Blade Optimization

Recently there has been some interest in applying optimization strategies to rotary wing aircraft design. However, most of these researchers[8-20] have addressed the problem in a sequential manner, based on individual disciplines, and attempts were made only to satisfy certain design requirements and criteria related to a single discipline. Such design procedures often lead to a final design that may not be the optimum solution when all disciplines are considered simultaneously. The rotary wing design process is truly multidisciplinary in nature and involves the coupling of several disciplines, such as structures, aerodynamics, dynamics, aeroelasticity and acoustics. For example, in an effort to reduce vibration by changing the mass and stiffness distributions of the blade, spanwise and/or chordwise, it is important to ensure that the aeroelastic stability of the rotor is not degraded. Also, while reducing the weight of the blade it is important to ensure that the rotor has sufficient autorotational inertia to autorotate in the case of an engine failure and that the rotor retains sufficient lifting capability. A proper formulation of the rotorcraft design problem therefore requires the coupling of all of these disciplines within the design optimization loop. The need to incorporate all of the necessary disciplines within a closed-loop optimization process is recently being recognized[21-31]. Brief descriptions of both the sequential and multidisciplinary optimization efforts follow.

Sequential Optimization: An early review of the literature in the area of application of optimum design techniques for helicopter rotor blades with dynamic constraints is due to Friedmann[7]. Successful applications of such techniques are presented in Refs. [8-20]. Bennett[9] addressed the problem of reducing the vertical hub shear transferred from the blade to the rotor mast by combining a conventional helicopter analysis with a nonlinear programming technique. Peters et al.[10] used two different objective functions at two stages of the design. Initially blade weight was used as the objective function which was later replaced by the difference between the actual and the desired natural frequency. A

simplified forced-response analysis was used, and a constraint was used on the autorotational inertia. More recently Chattopadhyay and Walsh[14,15] addressed the problem of optimum blade designs with dynamic constraints. Minimum weight designs were obtained with constraints on frequencies, stresses and autorotational inertia for articulated rotor blades with rectangular and tapered planforms. Weller and Davis[16] used a simplified rotor analysis code and quasisteady airloads to optimize rotor blades with dynamic and aeroelastic stability constraints. The results of Ref. [16] were verified by the authors through experimentation[17]. Walsh et al.[18] performed an aerodynamic/performance optimization using hover horsepower as the objective function with constraints on the horsepower required at five other flight conditions and the airfoil section drag coefficients. A combination of rotor horsepower in forward flight and hover was minimized by Kumar and Bassett[19] to obtain optimum rotor geometry for a future light helicopter. A preliminary structural optimization of rotor blades was conducted by Nixon[20]. Blade weight was used as the objective function and constraints were imposed on twist deformation, stresses and autorotational inertia.

Multidisciplinary Optimization: The necessity of integrated multidisciplinary optimization procedure for rotary wing design is currently being recognized. Celi and Friedmann[21] addressed the coupling of dynamic and aeroelastic criteria with quasisteady airloads for blades with straight and swept tips. Lim and Chopra[22] coupled a comprehensive aeroelastic analysis code with the nonlinear optimization algorithm CONMIN[32] to reduce all of the six 4/rev hub loads of a hingeless four-bladed rotor in order to reduce vibration without compromising aeroelastic stability in forward flight. However in these studies, only quasisteady airloads were used. A truly integrated aerodynamic/dynamic optimization procedure was presented by Chattopadhyay et al.[23]. The 4/rev vertical shear and blade weight of a four-bladed articulated rotor were minimized. A modified Global Criteria approach was used to formulate the multiobjective optimization

problem. The integration of aerodynamic loads and dynamics was achieved by coupling the comprehensive helicopter analysis code CAMRAD[33] with CONMIN and an approximate analysis technique. The program CAMRAD permitted the calculation of actual airloads. Its use within the optimization loop allowed for the effects of design variable changes, during optimization, and the associated changes in airloads to be included in the design process. Chattopadhyay and Chiu[24] extended the work of Ref. [23] to include the remaining critical vibratory forces and moments in the form of objective functions and/or constraints A combined structural, dynamic and aerodynamic optimization of rotor blades was performed by He and Peters[25]. A simple box beam model was used to represent the structural component in the blade and the blade performance was optimized using the power required in hover as the objective function. Constraints were imposed on natural frequencies, blade stress and fatigue life. However, the optimization procedure was decoupled into two levels. Straub et al.[26] addressed the problem of combined aerodynamic performance and dynamic optimization at both forward flight and hover flight conditions by using the comprehensive rotor analysis code CAMRAD/JA[34]. A linear combination of the objective functions was used to formulate the multiple design objective problem.

High-Speed Rotorcraft Design Considerations

High-speed rotorcraft designs, such as the tilting rotor configuration, pose an entirely new problem in the rotary wing field. The design goals for this class of aircraft include low downwash velocity in hover, good low speed maneuverability and cruise speeds of 350 - 500 knots[35]. Several new concepts[36-39] have recently been proposed to meet these design goals. Extensive research performed in this field have led to the XV-15 research aircraft[40] and ultimately to the production of the V-22 Osprey tilting rotor for the US Navy.

The combined requirements of efficient high-speed performance of a fixed wing aircraft and good helicopter-like hover characteristics complicates the design process of

tilting high-speed proprotor aircraft. It is necessary to maintain good aerodynamic efficiency in high-speed axial flight without degrading hover efficiency. This often leads to conflicting design requirements. For example, improved efficiency in high-speed cruise demands high drag divergence Mach numbers which are normally associated with thin airfoils. This however, reduces the hover figure of merit by reducing C_T/σ. Therefore, to maintain the required thrust ceiling in hover, the rotor solidity has to increase. Also as the forward speed increases, helical tip Mach number limitations, which when large reduce the aerodynamic efficiency of the rotor, require a reduction in the rotor rotational velocity. Introducing blade sweep can alleviate this problem by reducing the effective chordwise Mach number, which allows for higher speeds, without reducing the rotor RPM. Therefore the proper design of proprotor blades capable of achieving the design objectives must consider the right combination of airfoil thickness and blade sweep in addition to other aerodynamic variables such as planform and twist.

High-Speed Rotorcraft Optimization

Over the last few years, there has been a revival of interest in VTOL aircraft capable of operating in fixed wing as well as rotary wing mode. Several studies have been performed[41-46] to study design trade offs between the two flight modes. For example, Johnson et al.[41] performed a detailed study on the performance, maneuverability and stability of high-speed tilting proprotor aircraft, including the XV-15 and the V-22. Liu and McVeigh[42] recently studied the use of highly swept rotor blades for high-speed tilt rotor use. However, formal optimization techniques were not applied. Recently an effort was initiated by Chattopadhyay and Narayan[43,44] to develop formal multidisciplinary optimization procedures for the design of civil high-speed tilting proprotor blades. The propulsive efficiency in axial flight was maximized with constraints on the figure of merit in hover, aeroelastic stability in cruise and other aerodynamic and structural design criteria. McCarthy and Chattopadhyay[45] furthered this work by using multiobjective function

formulation techniques with the propulsive efficiency in cruise and the hover figure of merit as the individual objective functions to be maximized. Constraints were again imposed on the aeroelastic stability in cruise as well as on other structural design criteria such as the total blade weight.

Multiple Design Objectives

Multiobjective optimization refers to problems where the objective function is composed from a set of distinct criterion. For example in a structural design problem these may be stresses, displacements, weight, etc. As optimization is emerging as a practical design tool in the rotary wing industry and the need for multidisciplinary coupling is being recognized, multiobjective decision making is becoming an important issue. Therefore, there is a renewed interest in multicriteria programming for application to design problems. Following is a brief description of the current state of the art in multiobjective optimization.

The first concepts of multiobjective optimization date back to Pareto[46] who introduced the concept within the framework of welfare economics. Most applications of these problems in structural and mechanical designs are based on an ordering of the objective functions, prior to optimization, with the introduction of weight functions[47-50]. These techniques are, however, judgmental in nature as the weight factors rely heavily on the designer's experience and are often hard to justify. Also, in the highly nonlinear environment of rotary wing design, such techniques are often not well posed.

The use of multicriteria design techniques was recently studied by Chattopadhyay and McCarthy[27-31] for application to helicopter rotor blade design. In Ref. [27], the Minimum Sum Beta[16] (Min $\Sigma\beta$) and the Kreisselmeier-Steinhauser (K-S) function[51] approaches were used to reformulate the multiobjective function problem of Ref. [24]. The results from these two approaches were compared to the results from the modified Global Criteria approach as implemented in the original work. This work was extended in Ref. [28] by introducing additional discipline coupling. Also, the "generic" design variables such as

stiffnesses, used in Ref. [23,24,27] were replaced by a detailed structural modeling of the principal load carrying member in the blade. The Min $\Sigma\beta$ and the K-S function approaches were used to formulate the multiple objective function problem.

II. Objectives

The scope of the present work is threefold. Since most multidisciplinary optimization problems involve multiple design objectives, the formulation of such problems is investigated initially. The methods studied are applied to a helicopter rotor blade optimization problem. Next, using these multiobjective formulation techniques, a fully integrated dynamic/aerodynamic/structural/aeroelastic optimization procedure is developed for the design of helicopter rotor blades. In the last part of the thesis, such multidisciplinary optimization techniques are applied to study the complex design issues in high-speed tilting proprotor aircraft.

III. Multiobjective Optimization

A typical optimization problem involving multiple objective functions can be mathematically posed as follows.

Minimize	$F_k(\phi_n)$	$k = 1, 2, \ldots, NOBJ$	(objective functions)
		$n = 1, 2, \ldots, NDV$	
Subject to			
	$g_j(\phi_n) \leq 0$	$j = 1, 2, \ldots, NCON$	(inequality constraints)
	$\phi_{n_L} \leq \phi_n \leq \phi_{n_U}$		(side constraints)

where NOBJ denotes the number of objective functions, NDV is the number of design variables and NCON is the total number of constraints. The subscripts L and U denote lower and upper bounds, respectively, on the design variable ϕ_n. A detailed description of the multicriteria design objective formulation follows.

This study examines three multiobjective function formulation techniques that are less judgmental than the Pareto-based weight factors and are therefore more suited to large scale, highly nonlinear optimization problems that are associated with rotary wing design. The three multiobjective function techniques used are the modified Global Criteria, the Minimum Sum Beta (Min $\Sigma\beta$) and the Kreisselmeier-Steinhauser (K-S) function approaches. A detailed description of all three of the methods used follows.

Modified Global Criteria Approach

This approach was used by Chattopadhyay et al.[24] to formulate the two objective function problem studied in the original work, and is presented here for the sake of comparison. Using this method, each of the original objective functions is optimized individually. The optimum solution is then obtained by minimizing a "global criterion" defined as the sum of the squares of the relative deviations of the individual objective functions from their respective individually optimized values. Due to the nonlinearities

associated with a simple sum of the squares formulation, the square root of the summation is taken. The optimization problem reduces to minimizing the single global objective function, $\tilde{F}_1(\Phi)$, where

$$\tilde{F}_1(\Phi) = \sqrt{\sum_{k=1}^{NOBJ}\left[\frac{F_k(\phi)-F_k(\phi_k^*)}{F_k(\phi_k^*)}\right]^2} \tag{1}$$

subject to the complete set of inequality constraints

$$g_{1_j}(\Phi) \leq 0 \quad j = 1, 2, \ldots, NCON. \tag{2}$$

Side constraints are imposed on the design variables (Φ) to keep them in a practical range. The design variable vectors Φ_k^* are obtained by individually minimizing the single objective function $F_k(\Phi)$ subject to the set of constraints $g_{1_j}(\Phi)$, such that NOBJ optimizations of the original objective functions must be performed prior to the implementation of the modified Global Criteria approach.

Minimum Sum Beta (Min Σβ) Approach

This method was first used by Weller at al.[16] to formulate a two objective function rotor vibration problem. This method is a further modification of the Global Criterion approach in which the individually optimized values $F_k(\Phi_k^*)$ are replaced by specified target values. These prescribed values are analogous to the individually optimized values of the Global Criterion approach; however, these values represent user supplied information. The objective function, $\tilde{F}_2(\Phi)$, is defined as a linear combination of the tolerances of each objective function to its specified target value.

$$\tilde{F}_2(\Phi) = \sum_{k=1}^{NOBJ}\beta_k \tag{3}$$

where β_k are pseudo design variables with properties such that the original objective functions F_k remain within a β_k tolerance of some prescribed values. This requirement introduces new constraints of the following form.

$$\frac{F_k - \bar{F}_k}{\bar{F}_k} \leq \beta_k \qquad k = 1, 2, \ldots, NOBJ \tag{4}$$

The quantities $\bar{F}_k$ are the prescribed target values of the individual objective functions F_k. Using the above formulation, as the values of variables β_k are reduced to zero the values of the individual objective functions F_k are driven to their prescribed values, $\bar{F}_k$. The design variables for the Min $\Sigma\beta$ formulation comprise the original set of design variables and the pseudo design variables, β_k. A new constraint vector, $g_{2_m}(\Phi)$, m = 1, 2, ... , M, is also defined and this constraint vector comprises the original constraints and the new constraints presented in Eqn. 4, i.e., M = NCON + NOBJ.

Kreisselmeier-Steinhauser (K-S) Function Approach

This technique was first utilized by Sobieski et al.[51] at the NASA Langley Research Center. The first step in formulating the objective function in this approach involves transformation of the original objective functions into reduced objective functions[52]. These reduced objective functions take the form

$$F_k^*(\Phi) = \frac{F_k(\Phi)}{F_{k_o}} - 1.0 - g_{max} \leq 0 \qquad k = 1, \ldots, NOBJ \tag{5}$$

where F_{k_o} represents the value of F_k calculated at the beginning of each iteration. The quantity g_{max} is the value of the largest constraint corresponding to the design variable vector Φ and is held to be constant for each iteration. These reduced objective functions are analogous to the previous constraints, and therefore a new constraint vector $g_{3_m}(\Phi)$, m = 1, 2, ... , M, is introduced, where M = NCON + NOBJ. This constraint vector

includes the original constraints of the problem as well as the constraints introduced by Eqn. 5. The new objective function to be minimized is then defined, using the K-S function as follows:

$$\tilde{F}_3(\Phi) = f_{max} + \frac{1}{\rho} \ln \sum_{m=1}^{M} e^{\rho(g_m(\phi) - f_{max})} \tag{6}$$

where f_{max} is the largest constraint corresponding to the new constraint vector, $g_{3_m}(\Phi)$, and in general is not equal to g_{max}. The optimization procedure is as follows. Initially in an infeasible design space, where the original constraints are violated, the constraints due to the reduced objective functions (Eqn. 5) are satisfied (g_{max} is negative). Once the original constraints are satisfied, the constraints due to the reduced objective functions become violated. When this happens, the optimizer attempts to satisfy these constraints and in an effort to do so, so minimizes the original objective functions (F_k). The multiplier ρ is analogous to a draw-down factor where ρ controls the distance from the surface of the K-S objective function to the surface of the maximum constraint function. When ρ is large the K-S function closely follows the surface of the largest constraint function. When ρ is small the K-S function includes contributions from all violated constraints. The design variable vector Φ is identical to that used in the Global Criteria approach.

Problem Statement

The objective is to evaluate the different multiobjective formulation techniques described above. This is accomplished by reformulating the multicriteria objective function formulation of Ref. [24] in which the objective function was formulated using the modified Global Criteria approach. The two new techniques, the Min $\Sigma\beta$ and the K-S function approaches are used. As in the original study both structural and aerodynamic design variables are used to study the trade off between dynamic and aerodynamic performance

requirements. The objectives are to reduce the critical vibratory hub loads, without incorporating weight penalties or degrading the lifting capability of the rotor.

Blade model

The reference rotor, as used in Ref. [24], is a modified wind tunnel version of the Growth Black Hawk rotor blade[53], which is a four bladed articulated rotor. For convenience a description of the blade model as used by Chattopadhyay et al.[23] is given below. The blade planform is modeled with linear taper (Fig. 1), and the blade stiffnesses are assumed to be contributed entirely by the blade structural components (i.e. the stiffnesses contributed by the skin, the honeycomb, etc., are assumed to be negligible). The blade is assumed to have a linear twist distribution with a tip twist value of -16 degrees.

$$\tilde{\lambda} = \frac{c_t}{c_r}$$

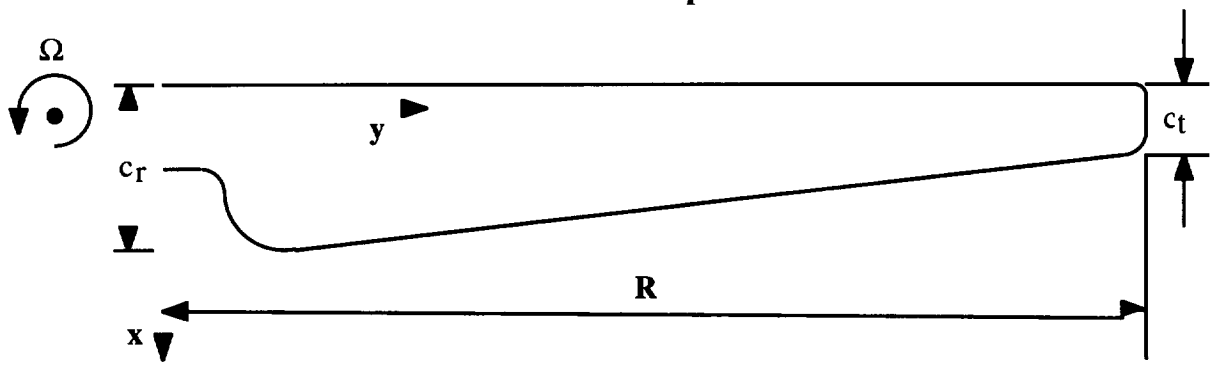

Figure 1 Simplified rotor blade model with linear taper

The linear chord distribution is given as

$$\tilde{c}(y) = \frac{c(y)}{c_r} = [\bar{y}\,(\tilde{\lambda} - 1) + 1] \tag{7}$$

where c_r is the root chord, $\bar{y}$ is the nondimensional radial location ($\bar{y} = y/R$, where R is the blade radius) and $\tilde{\lambda}$ is the inverse taper ratio, i.e. $\tilde{\lambda} = c_t/c_r$ where c_t is the tip chord. Note

that when $\tilde{\lambda} = 0$ the planform is triangular. The mean chord, c_e , is found from the weighted average of the chord length at each node as follows

$$c_e = \frac{1}{R} \sum_{i=1}^{NSEG} L_i \bar{c}_i \tag{8}$$

where NSEG represents the total number of segments in the discretized blade, L_i is the length and $\bar{c}_i$ the average chord of the i^{th} segment, respectively. Based on the above chord distribution and the fact that moments of inertia are proportional to $[L]^4$, the stiffness EI_{xx} is represented as follows.

$$\bar{EI}_{xx}(y) = \frac{EI_{xx}(y)}{EI_{xx_r}} = [\bar{y}\,(c(\bar{y}) - 1) + 1]^4 \tag{9}$$

where E is Young's modulus and I_{xx} is the moment of inertia about the x-axis. Similar expressions are obtained for the lagging stiffness EI_{zz} and the torsional stiffness, GJ, where G is the torsional rigidity and J is the polar moment of inertia. The total blade weight is formulated as follows

$$W_i = \sum_{i=1}^{NSEG} \left(w_{s_i} + w_{ns_i} \right) \tag{10}$$

where W_{s_i} and W_{ns_i} refer to the structural and nonstructural weights, respectively, of the i^{th} segment. The structural weight of each segment is represented as

$$W_{s_i} = \rho\, A_i\, L_i \tag{11}$$

where A_i the average area of the i^{th} segment and ρ is the density. Because the structural weight is dependent upon the cross-sectional area it is necessary to estimate the cross-

sectional area of each segment. This is done by formulating the area in terms of the blade stiffnesses and radius of gyration as

$$A = \frac{(EI_{xx} + EI_{zz})}{Ek^2} \tag{12}$$

where k is the principal radius of gyration given by

$$k^2 = k_{xx}^2 + k_{zz}^2 \tag{13}$$

The nonstructural weights (per unit length), w_i , are specified at each node point. The total nonstructural weight of each segment is then formulated as the average of the nonstructural weights per unit length at adjacent node points multiplied by the length of the segment as follows.

$$W_{nsi} = L_i\left[\frac{w_i + w_{i+1}}{2}\right] \qquad i = 1, 2, ..., NSEG \tag{14}$$

The autorotational inertia, AI, is formulated from the blade weights as follows.

$$AI = \sum_{i=1}^{NSEG} W_i \hat{y}_i^2 \tag{15}$$

Where W_i is the total weight of the i^{th} segment and $\hat{y}_i$ represents the length from the blade root to the center of the i^{th} segment. The centrifugal stress, σ_i, of the ith segment is then calculated as

$$\sigma_i = \frac{\sum_{j=1}^{NSEG} W_j \omega^2 \hat{y}}{A_i} \qquad i = 1, 2, ..., NSEG \tag{16}$$

where ω is the rotational velocity of the rotor blade in rad/sec.

Optimization

Objective Functions: For a four-bladed rotor, often the 4/rev vibratory vertical shear at blade root is not the only critical source of hub vibration. Depending upon the hub impedance and other factors, the contributions from the 3/rev and 5/rev harmonics often become significant. Therefore, in this problem the objective functions used are the 4/rev vertical shear (f_z) and the 3/rev inplane shear (f_x) at the blade root.

Design Variables: For the optimization procedure, both aerodynamic and structural design variables are used in order to provide additional flexibility to the optimization process. Following, is a summary of the design variables used.

(i) Chord distribution parameters; c_r, $\tilde{\lambda}$

(ii) Blade stiffnesses at the root; EI_{xx_r}, EI_{zz_r} and GJ_r

(iii) Radius of gyration at the root; k_r

(iv) Nonstructural weights; w_j; $j = 1, 2, \ldots, NSEG$

Dynamic Criteria: In this problem, the optimum design of the rotor blade under forward flight condition is addressed with the objective of minimizing the critical vibratory forces and moments at the blade root. As mentioned before, the rotor being four-bladed, the 4/rev vertical shear and the 3/rev inplane shear at the blade root, are used as objective functions. However, to ensure that there is no degradation of the remaining critical vibratory forces, upper bound constraints are imposed on these forces and moments. Also to avoid resonance, upper and lower bounds, or "window" constraints, are placed on the first four elastic coupled flap and lead-lag natural frequencies of the blade. This ensures that the blade natural frequencies are away from integer harmonics of the rotor. These constraints are formulated as follows

(i) 3/rev radial shear; $f_r \leq f_{rU}$

(ii) 4/rev lagging moment; $m_z \leq m_{zU}$

(iii) 4/rev flapping moment; $m_x \leq m_{xU}$

(iv) 4/rev torsional moment; $m_c \leq m_{cU}$

(v) first four elastic coupled lead-lag natural frequencies;

$f_{iL} \leq f_i \leq f_{iU}$ i = 3, . . ., 6 (the first two modes, i = 1,2, represent rigid body modes.)

Aerodynamic Criteria: In order to make a meaningful comparison between the optimum and reference rotors it is necessary that the optimum rotor has at least the same lifting capability as the reference rotor. Therefore, a lower bound is imposed on the total rotor thrust. This constraint takes the following form .

(vi) $T \geq T_L$

Structural Criteria: Most conventional vibration reduction problems are associated with increased weight due to the addition of tuning masses and/or vibration isolators. To avoid such a weight penalty, an upper bound is imposed on the total blade weight, W. A lower bound is imposed on the autorotational inertia of the blade (AI) in order to ensure that the blade has sufficient autorotational inertia to autorotate in the case of engine failure. Further, it is necessary that the blade is capable of withstanding the centrifugal stresses from its rotation, therefore upper bounds are placed on the blade centrifugal stress (σ_i, i = 1, 2, ..., NSEG). Details of the structural constraints follow.

(vii) $W \leq W_U$

(vii) $AI \geq AI_L$

(vii) $\sigma_i \leq \sigma_{al}$ i = 1, 2, ... , NSEG

Analysis

Dynamic, Aerodynamic and Aeroelastic Analyses: The program CAMRAD is used for both blade dynamic and aerodynamic analyses. Since the reference blade is a wind tunnel

blade model, the wind tunnel option within CAMRAD is used for all of the problems studied. The blade is trimmed, within CAMRAD, at each cycle of design optimization. This ensures that the intermediate designs, which are feasible, represent trimmed configurations. The rotor lift and drag, each normalized with respect to solidity, and the flapping angle are trimmed using the collective pitch, the cyclic pitch and the shaft angle in the helicopter rotor blade optimization. The optimum rotor is trimmed to the (C_T/σ) value of the reference blade, where C_T represents the rotor thrust coefficient and σ is the area-weighted solidity of the rotor. A Galerkin approach is used within CAMRAD to solve the dynamic equations of motion and the aerodynamics are based on lifting line theory with unsteady and yawed flow corrections with the assumption of uniform inflow.

Structural Analysis: For this problem the structural properties throughout the span are calculated based on the "generic" stiffnesses at the root and the chord distribution (Eqns. 7-16).

Optimization Implementation

Optimization Algorithm: The optimization is performed by using the program CONMIN. The program uses the method of feasible directions to solve non-linear constrained optimization problems.

Sensitivity Analysis: The optimization algorithm is based on the method of feasible directions and requires the first derivatives of the objective functions and the constraints. Due to the complexity and the nonlinearity of the rotary wing analysis procedure, these gradients are calculated using a forward finite difference approximation with a step size of 0.1 percent of each design variable.

Approximation Techniques In the optimization process, several evaluations of the objective function and the constraints are required before convergence to an optimum

design is achieved. In large scale optimization problems, such as the rotary wing blade design problem, this process becomes computationally prohibitive if exact analyses are performed for every function evaluation. Therefore, an approximate analysis technique is used to provide this information during intermediate steps within CONMIN. For this problem, a simple first order linear Taylor series-based expansion is used.

The objective function, $F(\Phi)$, and the constraint function, $g_m(\Phi)$, are approximated using the first order Taylor series as follows

$$\hat{F}(\Phi) = F(\Phi_o) + \sum_{n=1}^{NDV} \frac{\partial F(\Phi_o)}{\partial \phi_n} \Delta\phi_n \tag{17}$$

and

$$\hat{g}_m(\Phi) = g_m(\Phi_o) + \sum_{n=1}^{NDV} \frac{\partial g_m(\Phi_o)}{\partial \phi_n} \Delta\phi_n \qquad m = 1,2, \ldots, M \tag{18}$$

where ϕ_n is the n^{th} design variable vector, $\Delta\phi_n$ is the corresponding incremental difference in the design variable vector, NDV is the number of design variables and M denotes the total number of constraints. The quantities $\hat{F}(\Phi)$ and $\hat{g}_m(\Phi)$ represent the approximate values of the objective function and the constraint, respectively. The first order expansion assumes that the functions are linear, which is valid only for very small intervals. Therefore a "move limit" defined as the maximum fractional change of each design variable[23], is introduced as an upper and lower bound on $\Delta\phi_n$. The procedure is associated with a trade-off between a more accurate but slower convergence to a minimum due to a small move limit and a faster convergence along with the possibility of missing an optimum point due to a larger move limit. A variable move limit procedure is therefore used. Initially larger movements of the order of 10 - 25 percent of the design variable values are

used to converge to point near a local minimum, then move limits as small as 0.1 percent of the design variable are used to converge smoothly to the optimum design.

Results and Discussions

The blade model studied for this problem is a wind tunnel model of a modified Growth Black Hack rotor blade which has a radius, R = 4.685 ft. and a rotational velocity, 639.5 RPM (revolutions per minute). Optimization is performed in the forward flight condition with an advance ratio, $\mu = 0.3$. Titanium is used for the structural modeling. The blade model is discretized into 6 segments (NSEG = 6), therefore, for the modified Global Criteria and the K-S function approaches 12 design variables are used. For the Min $\Sigma\beta$ approach 14 design variables are used which includes the 2 pseudo design variables. Due to the high degree of nonlinearities present in the objective functions and the constraints, the move limits used in the approximation procedure are carefully monitored. Often very small move limits of the order of 0.1 - 1.0 percent are used which lead to an increase in the convergence time in the Min $\Sigma\beta$ case.

Tables 1 and 2 present summaries of the constraints used. Table 1 indicates that all four elastic modes (f_3 - f_6) and the autorotational inertia (AI) are at their prescribed upper bounds in the K-S case. The frequency f_6, corresponding to the first elastic lead-lag dominated mode, is active in the Global Criteria formulation. The weight constraint is active in the Min $\Sigma\beta$ and the K-S cases, whereas the blade weight reduces by 0.6 percent in the Global Criteria approach. The thrust constraint is active in all three cases. Figure 2 presents the distribution of the centrifugal stresses along the blade span (prescribed $\sigma_{max} = 25 \times 10^6$ lb/in^2), and indicates reductions of these stresses from the reference blade values. The most significant reductions occur in the Global Criteria and the K-S cases.

Table 2 presents a summary of the reference blade and the optimized blade design variables (except for the nonstructural masses). All of the design variables, with the exception of k_r (the radius of gyration) and the nonstructural masses, remain unchanged in the Global Criteria approach from the reference to the optimum. Substantial changes occur in both the Min $\Sigma\beta$ and the K-S cases. For example, the root chord c_r is reduced by 4.4 percent in the Min $\Sigma\beta$ case and by 21.8 percent in the K-S case. The planform remains uniform after optimization ($\tilde{\lambda}$ = 1.0) using the Global Criteria approach, whereas optimization produces an "inverse taper" (i.e. larger tip chord relative to the root chord) with $\tilde{\lambda}$ = 1.04 in the Min $\Sigma\beta$ case and $\tilde{\lambda}$ = 1.33 in the K-S case (the prescribed upper limit).

Table 1 Summary of Multiobjective Optimization Constraints

	Reference	Prescribed bounds		Optimum		
		lower	upper	Global	Min $\Sigma\beta$	K-S
f_3 (per rev) (flap)	3.07	3.05	3.50	3.13	3.15	3.05
f_4 (per rev) (flap)	6.76	6.50	6.90	6.87	6.89	6.90
f_5 (per rev) (flap)	9.28	9.25	9.50	9.38	9.49	9.50
f_6 (per rev) (lead-lag)	12.63	12.50	12.75	12.75	12.68	12.75
AI (lb-ft^2)	19.75	19.75	-	20.30	22.53	19.75
W (lb)	3.41	-	3.41	3.39	3.41	3.41
3/rev f_r (lb)	2.71	-	2.81	2.65	2.285	2.35
3/rev m_x (lb -ft)	0.69	-	0.69	0.69	0.59	0.43
3/rev m_c (lb -ft)	0.24	-	0.24	0.24	0.21	0.22
4/rev m_z (lb -ft)	0.63	-	0.63	0.58	0.49	0.42
Thrust, T (lb-ft)	297.10	297.10	-	297.10	297.10	297.10
β_1	0.10	0.0005	0.1050	-	0.0074	-
β_2	0.10	0.0005	0.1050	-	0.0377	-

Table 2 Summary of Multiobjective Design Variables

	Reference	Optimum		
		Global	Min $\Sigma\beta$	K-S
EI_{xx_r} (lb-ft^2)	10277.0	10277.0	10605.9	8563.0
EI_{zz_r} (lb-ft^2)	354.0	354.0	326.5	290.7
GJ_r (lb-ft^2)	261.0	261.0	332.6	299.6
k_r (lb-ft^2)	0.27	0.16	0.17	0.11
$\tilde{\lambda}$	1.00	1.00	1.04	1.33
c_r (ft)	0.45	0.45	0.43	0.35

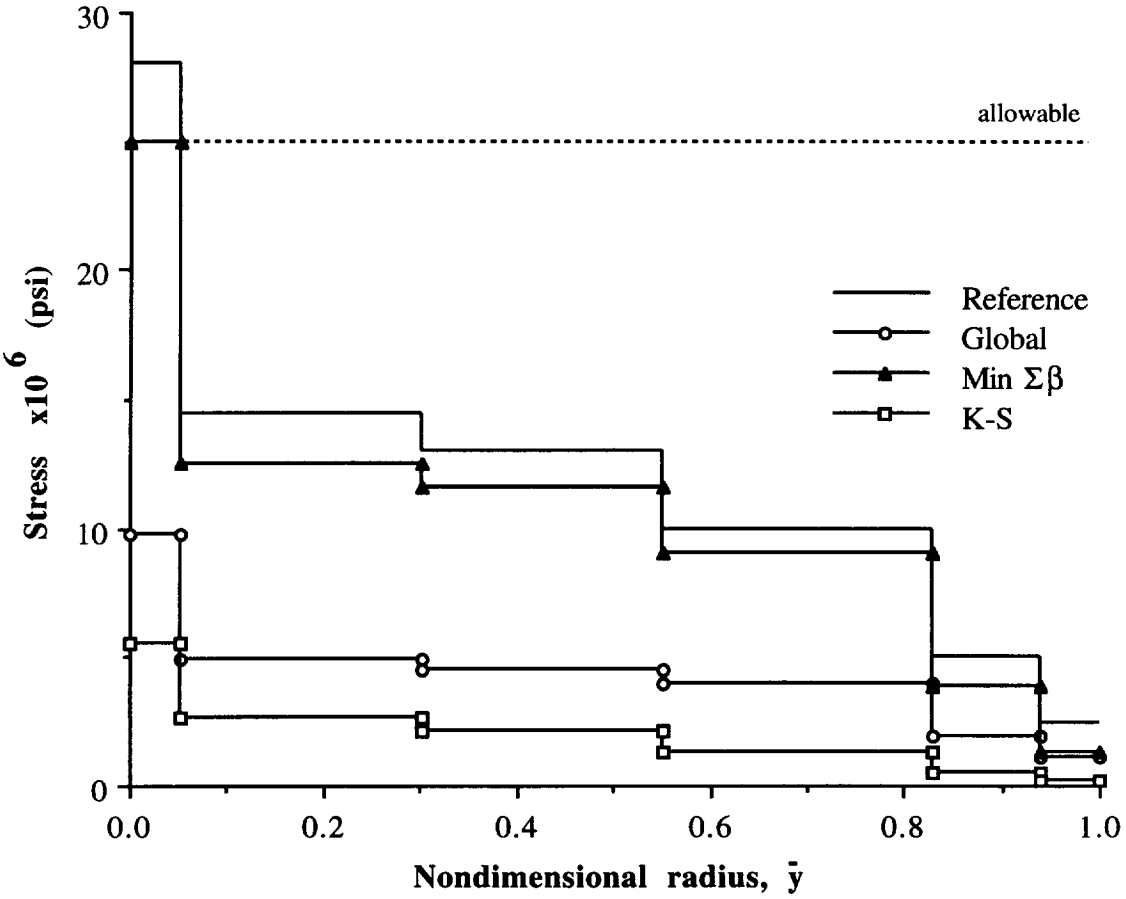

Figure 2 Centrifugal stress distribution

The bending stiffness EI_{xx} is plotted, along the blade radius, for the reference and the optimum blades in Figure 3. The figure shows a significant increase in the EI_{xx} value

towards blade tip for the optimum blade in the K-S case due to the increased tip chord. It is of interest to note that there is a substantial increase in the value of the root torsional stiffness, GJ_r, both in the Min $\Sigma\beta$ case (27.4 percent) and the K-S function case (14.8 percent).

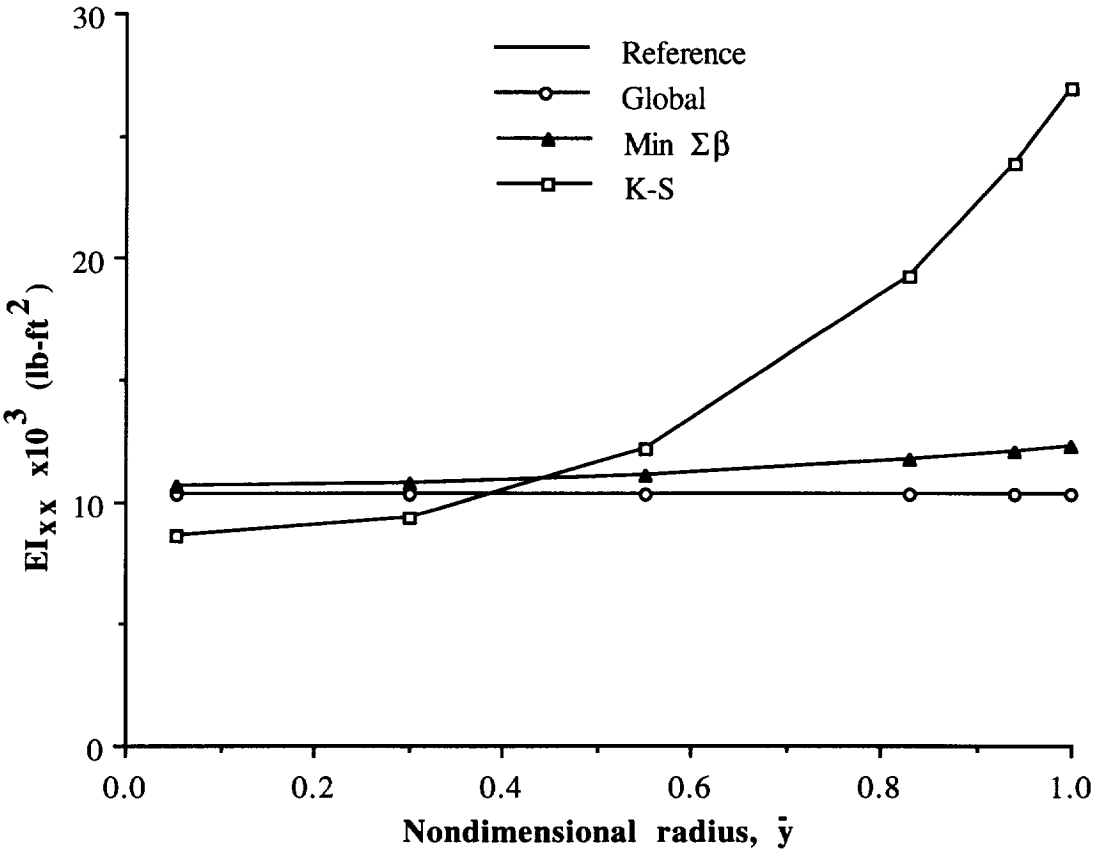

Figure 3 Lead-lag bending stiffness distribution

Figure 4 presents the nonstructural weight distributions of the reference and the optimum blades showing a significant change in these distributions. In the Global Criteria approach, the nonstructural weights of the optimum blade are lower (significantly towards blade inboard) than those of the reference throughout the entire span. In the Min $\Sigma\beta$ case, the nonstructural weights are greatly reduced towards blade inboard, but increase significantly towards outboard (50 - 90 percent of blade radius). This is due to the

autorotational inertia constraint which requires the total mass to be sufficient towards blade outboard. The corresponding distribution is significantly different in the K-S case, with greatly increased values at blade tip and significant reductions towards blade outboard. A possible explanation of this significant decrease towards blade outboard, is the relative increase in the blade structural weight towards outboard caused by the significant increase in the value of c_t in the K-S case. This causes a reduction in the nonstructural weights at those locations to satisfy the constraint on the total weight. The nonstructural weight at the tip is larger than that of the reference only in the K-S case.

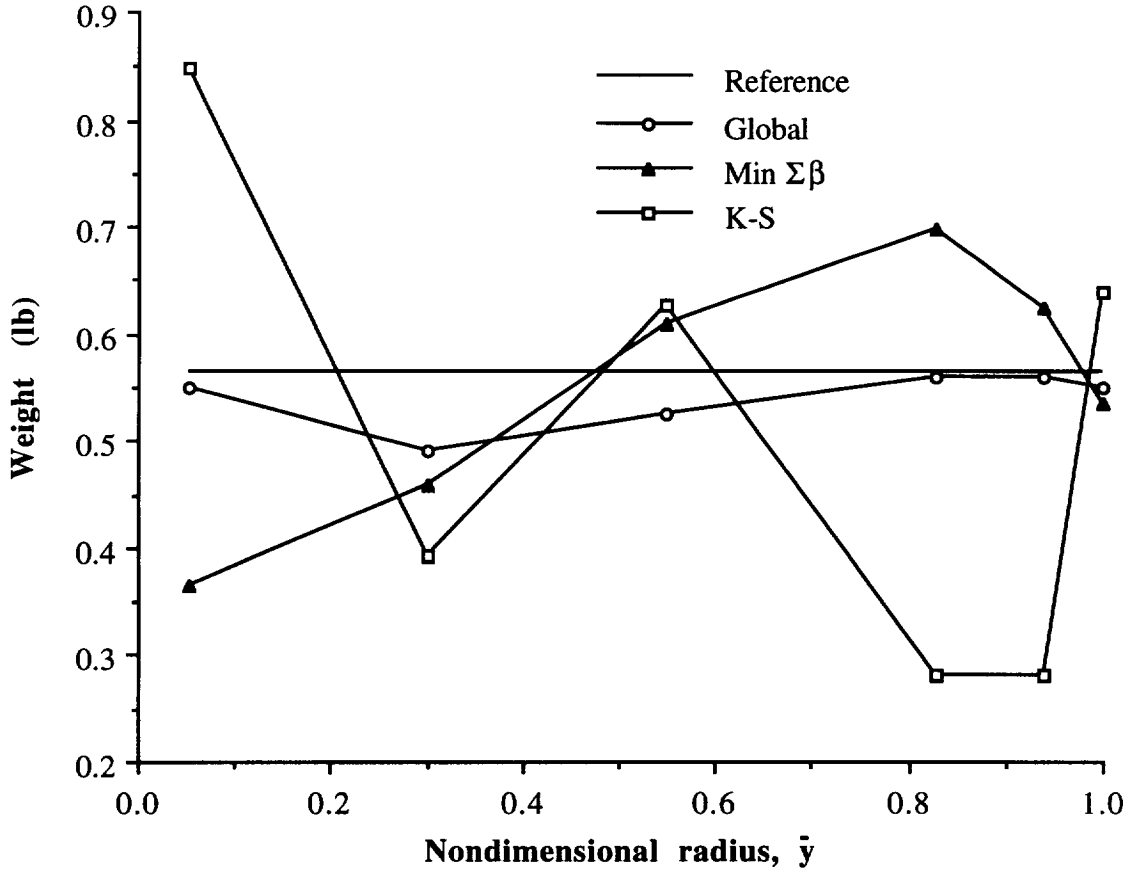

Figure 4 Nonstructural weight distribution

Figure 5 presents comparisons of the objective functions of the reference and the optimum blades. The most significant reductions in both the 4/rev vertical shear f_z (16.8 percent) and the 3/rev inplane shear f_x (16.5 percent) are achieved by using the K-S approach. The reduction in f_z is 10.9 percent in the Global Criteria case and 7.2 percent in the Min $\Sigma\beta$ case. The situation is reversed with f_x, the reduction being 4.10 percent in the Global Criteria case and 13.8 percent in the Min $\Sigma\beta$.

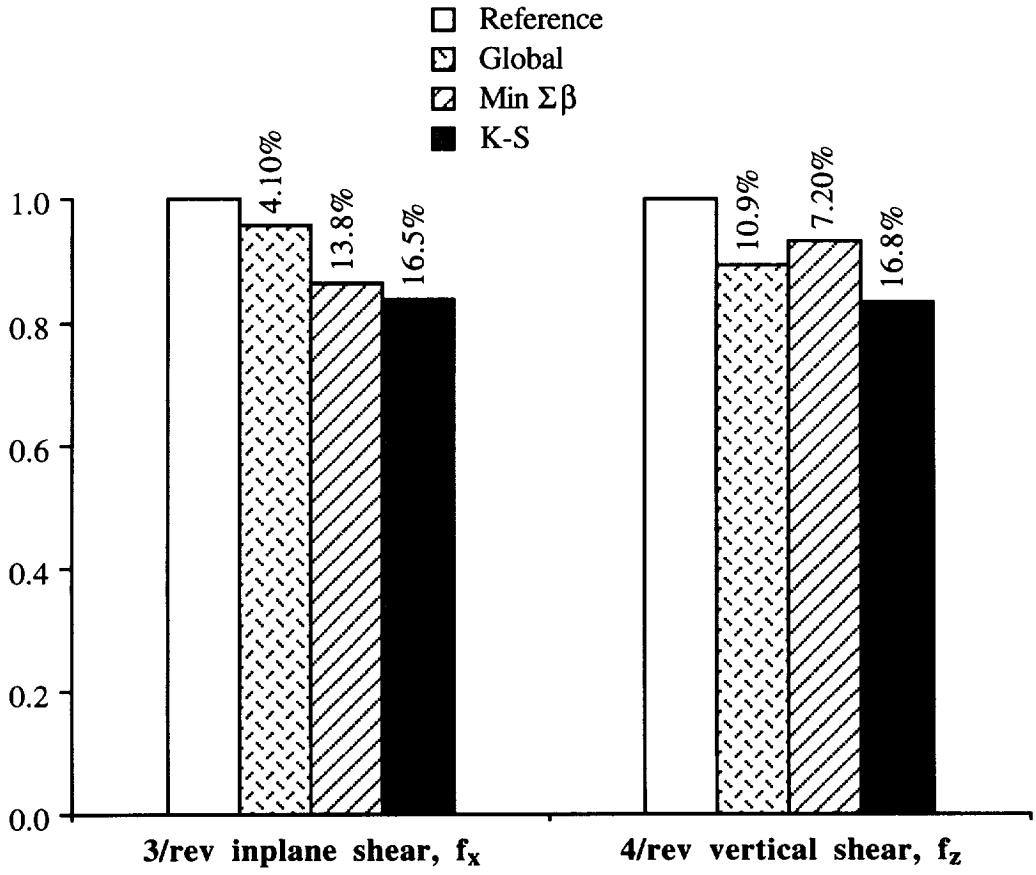

Figure 5 Comparison of individual objective functions

The convergence characteristics of the individual design objectives, f_z and f_x, are presented in Figures 6 and 7. Although the value of f_z is increased significantly (from the reference value) initially (Fig. 6), the convergence to the local minimum is achieved faster in the K-S function case than in the Min $\Sigma\beta$ case. This shows that the problem is well

formulated and the optimizer is working well to satisfy the constraints. When the constraints are all satisfied, the value of f_z is reduced significantly from the reference blade as well as the optimum value obtained from the Min $\Sigma\beta$ formulation. Similar observations are made on the second objective function, f_x (Fig. 7). It is to be noted that the individual objective functions do not exhibit the usual convergence expected from single objective function optimization, due to the fact that the optimization is based upon their combined convergence requirement.

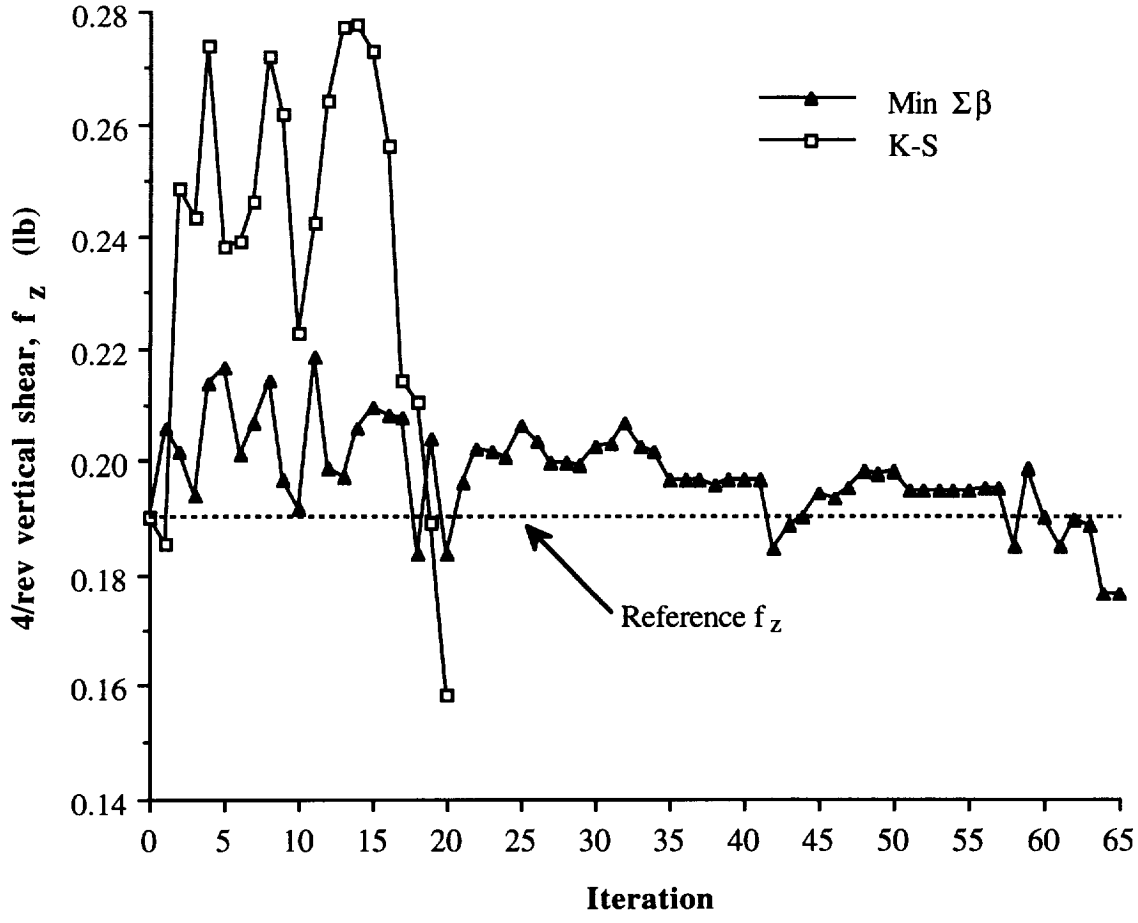

Figure 6 4/rev vertical shear iteration history

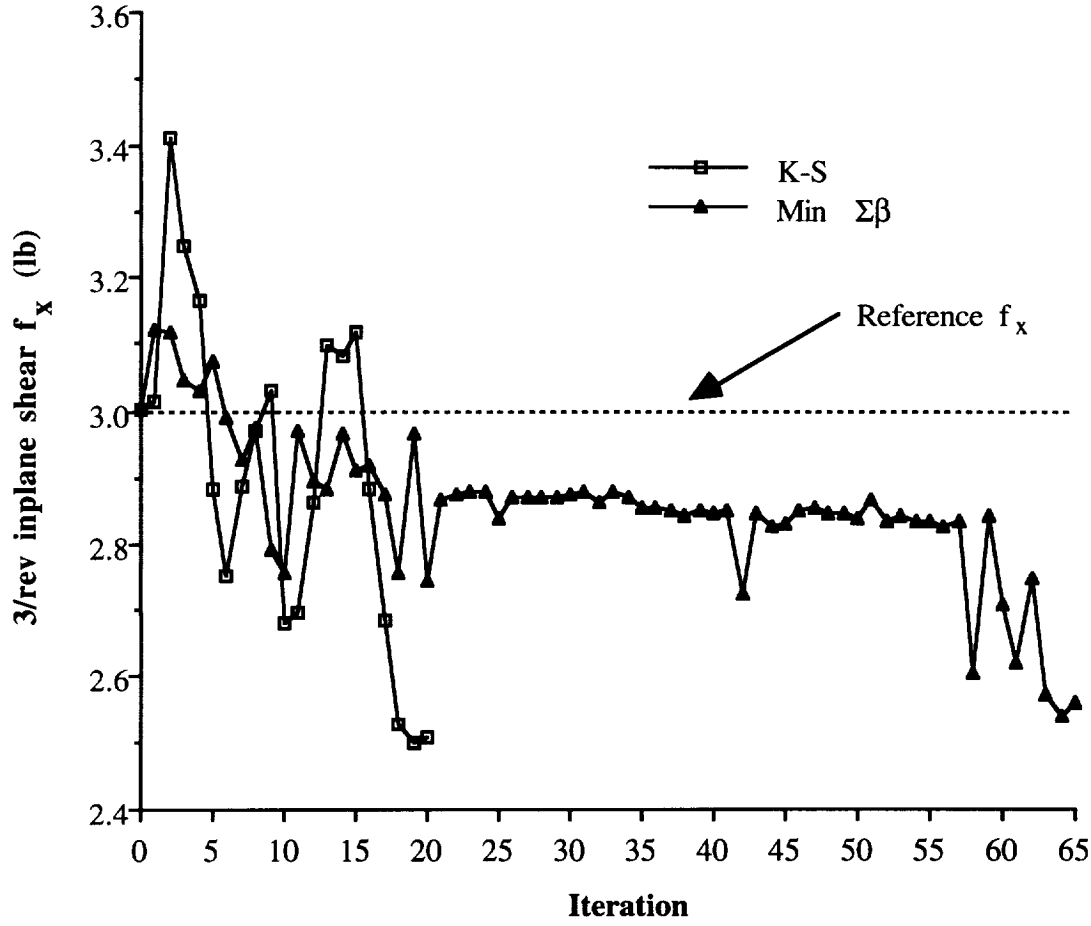

Figure 7 3/rev inplane shear iteration history

The convergence history of the overall objective functions, corresponding to the two new approaches presented in this paper, the Min Σβ and the K-S function approaches, are presented in Figure 8. The figure indicates a faster convergence in the K-S approach.

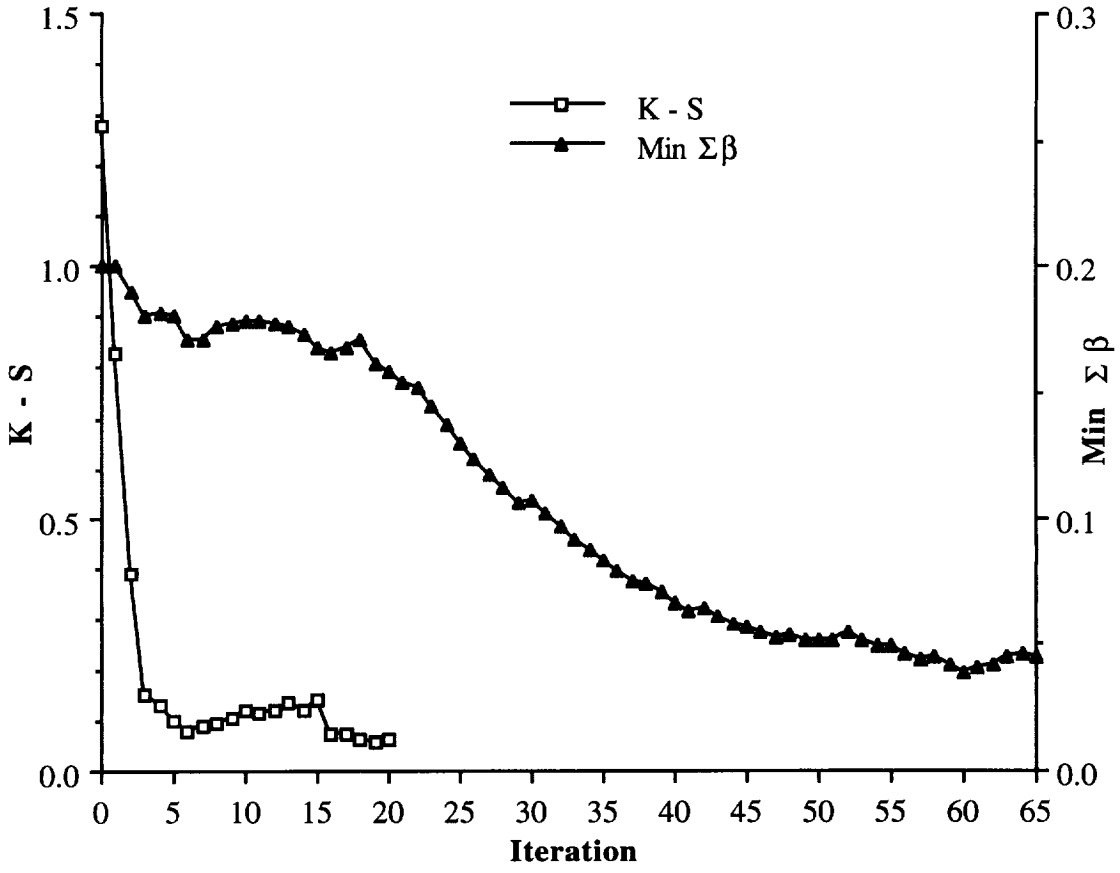

Figure 8 Objective function iteration history

Conclusions

The application of three different multiple objective optimization procedures are investigated for optimum design of helicopter rotor blades with the couplings of aerodynamics and dynamics. The 4/rev vertical and the 3/rev inplane root shears are minimized with constraints on remaining critical vibratory forces and moments, frequencies, autorotational inertia, and rotor thrust. The results obtained using the modified Global Criteria approach, the Min Σβ approach, and the K-S function approach

are compared with a reference blade design. The following conclusions are made from this problem.

1) All of the three optimization formulation procedures used, provided significant reductions in the objective function values, with the maximum reductions obtained by using the K-S function approach. The results obtained must, however, be treated within the context of the problem formulation and particularly the constraints imposed.
2) The Min $\Sigma\beta$ and the K-S function approaches were computationally more efficient since they did not require optimization of the individual objective functions.
3) The three approaches converged to three different local minima. The optimum blade was closer to the reference blade design in the Global Criteria approach and differed most significantly from it in the K-S function approach. The importance of properly selecting a multiobjective formulation technique is seen by examining the three radically different results.
4) The active constraints that influence the optimization most heavily in the Min $\Sigma\beta$ approach are the stress, the thrust and the lagging moment. These constraints remain active or nearly active through the entire optimization process. The driver constraint in the K-S function approach is the thrust.
5) Very small move limits were required in the Global Criteria approach (Ref. 24) and also in the Min $\Sigma\beta$ case due to the nonlinearities of the functions involved.
6) The K-S function approach was less judgmental and provided the fastest convergence. It did not require single objective optimizations as required by the Global Criteria approach, or specific target values of the objectives, as required by the Min $\Sigma\beta$ approach. Several values of the K-S factor ρ were tested and the value of $\rho = 200$ proved to be most effective in obtaining convergence.

V. Integrated Helicopter Rotor Blade Optimization

Problem Definition

In order to extend the state of the art in multiobjective optimization of helicopter rotor blades, the original problem of Ref. [24] is reformulated with additional design criteria using more realistic nonlinear chord and twist distributions. Also, a detailed structural model consisting of a two-celled box beam configuration (Fig. 9) is used to model the principal load-carrying members of the blade. The beam dimensions are used to replace the "generic" design variables used in Ref. [24]. The four-bladed modified Growth Black Hawk rotor blade is once again used as the reference rotor. The objective is to develop a fully integrated design procedure with the coupling of dynamic, aerodynamic, structural and aeroelastic design criteria. The Min $\Sigma\beta$ and the K-S function approaches are used to formulate the multiple design objective problem.

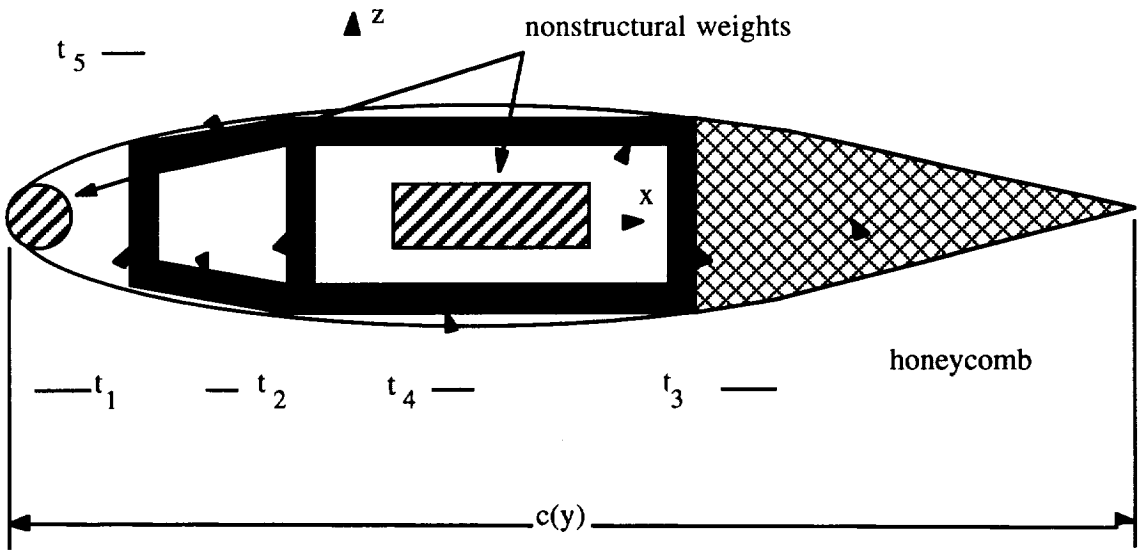

Figure 9 Double-celled box beam configuration

Blade Model

The load carrying structure of the rotor is modeled as a double-celled box beam that is symmetric about the x-axis (Fig. 9). The outer dimensions of the box beam are fixed percentages of the blade chord. The individual thicknesses of the webs and the flanges are linearly varied with the chord such that

$$t_i(y) = t_{i_r} \frac{c(y)}{c_r} \qquad i = 1, 2, \ldots, \text{NMEM} \tag{19}$$

where t_{i_r}, is the wall thickness of the i^{th} member of the box beam at the blade root.

The normalized chord distribution, $\bar{c}(y)$, is defined to have spanwise chord variation as follows

$$\bar{c}(y) = \frac{c(y)}{c_r} = [\bar{y}\,(\tilde{\lambda} - 1) + 1]\{1 - \bar{y}^{1/\alpha}\}^p \tag{20}$$

where $\tilde{\lambda}$ is again the inverse taper ratio. The tip shape parameter, denoted p, defines the blade shape at the tip and the tip length parameter, denoted α, defines the amount of tip taper. Both of these parameters are defined to be strictly positive and their physical significance is illustrated in Figs. 10 and 11 where it is seen that when p = 0.0, the blade has a rectangular planform (Fig. 10) and when p = 1.0, λ = 1.0 and α = 1.0 the blade is triangular (Fig. 11). The mean chord is calculated using Eqn. 8.

The blade twist angle, $\bar{\theta}(y)$, normalized with respect to the root twist θ_r, is defined to have the following spanwise variation

$$\bar{\theta}(y) = \frac{\theta(y)}{\theta_r} = 1 + \bar{y}^{\delta}(\tau - 1) \tag{21}$$

In the above equation, τ is the twist ratio, given by $\tau = \theta_t / \theta_r$, where θ_t is the tip twist and δ is the twist shape parameter which is defined to be positive. The physical significance of δ is shown in Fig. 12 which indicates that when $0 < \delta < 1$ the twist is concave and when $\delta > 1$ the twist is convex. The limiting case of $\delta = 1$ indicates linear twist.

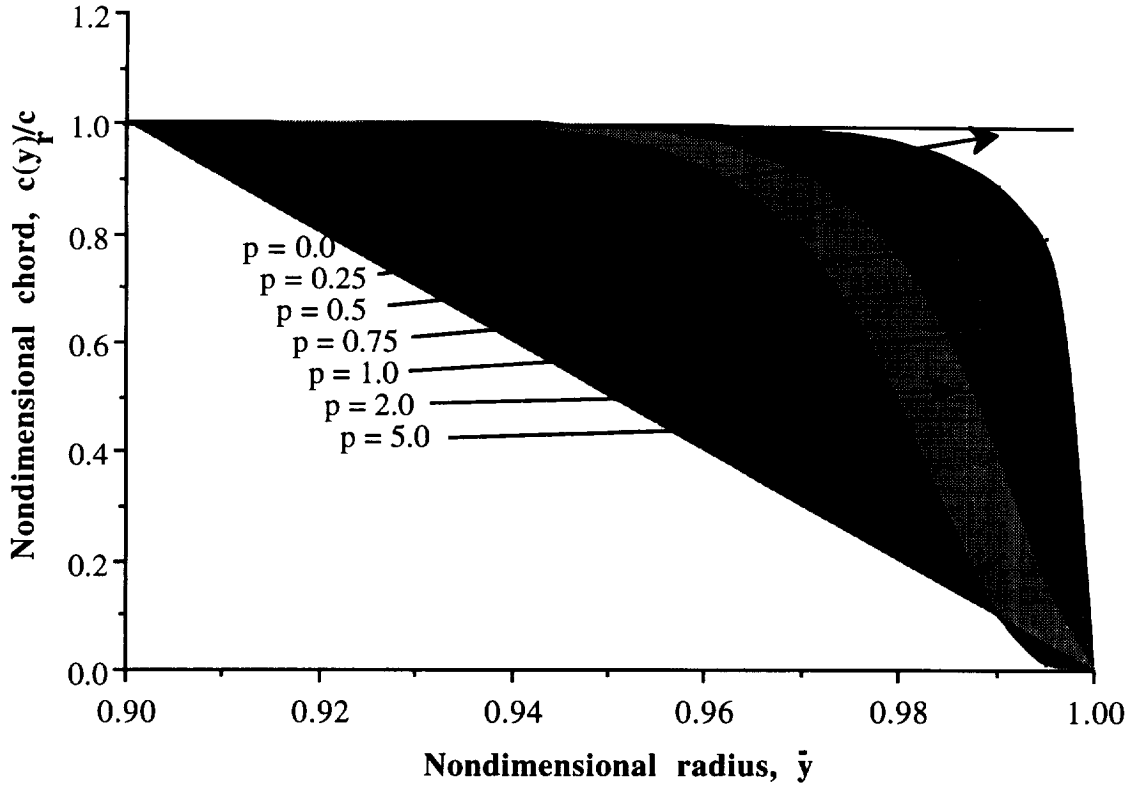

Figure 10 Variation of tip shape with tip shape parameter p, $\alpha = 0.001$ and $\lambda = 1.0$

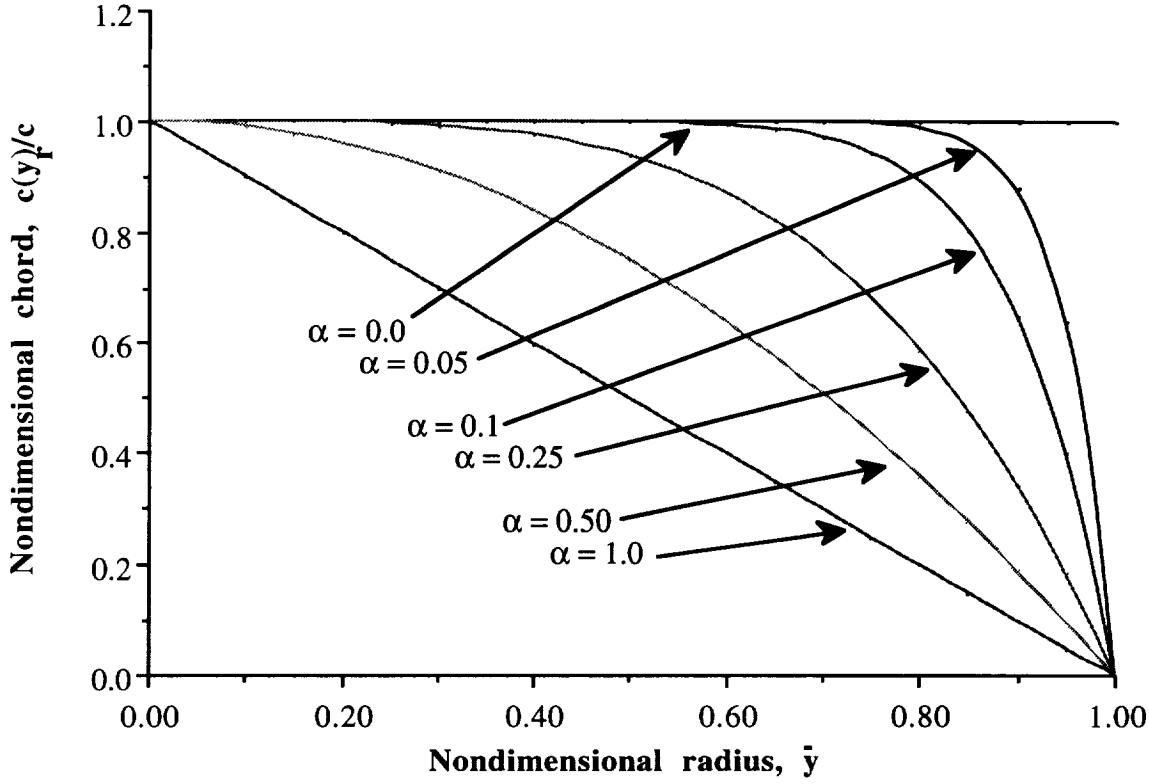

Figure 11 Variation of tip shape with tip shape parameter α, $p = 1.0$ and $\lambda = 1.0$

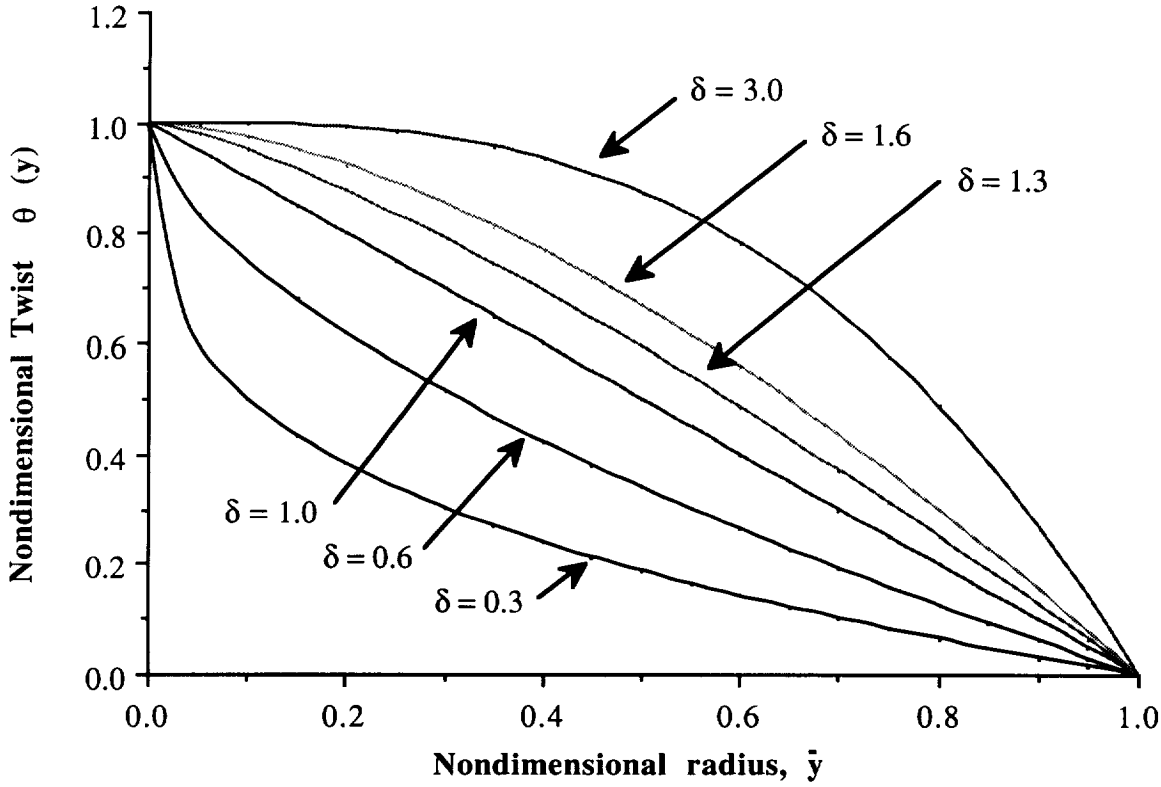

Figure 12 Variation of blade twist with changes in tip shape parameter, δ, ($\tau = 0.0$)

In this problem, nonstructural tuning masses are placed at both the center of the rectangular cell, w_c, and at the leading edge, w_t (see Fig. 9). The total nonstructural weight is then defined as

$$W_{ns_i} = L_i\left[\left(\frac{w_{c_i} + w_{c_{i+1}}}{2}\right) + \left(\frac{w_{t_i} + w_{t_{i+1}}}{2}\right)\right] \tag{22}$$

where w_{c_i} and w_{t_i} are nonstructural weights per unit length. The blade nonstructural weight, w_{ns_i}, and the total blade weight, W, are calculated using Eqns. 11 & 14, respectively. The calculation of the autorotational inertia and centrifugal stresses follow Eqns. 15 and 16, respectively.

In the present problem, both vibratory and centrifugal stresses are considered and the total blade stress, σ, is calculated as

$$\sigma = \sigma_{cent} + \sigma_{vib} \tag{23}$$

where σ_{cent} is centrifugal stress component and σ_{vib} is vibratory stress component. The vibratory stress is calculated at each of the six corners of the beam as follows.

$$\sigma_{vib} = \frac{f_r}{A} - \frac{m_x z}{I_{xx}} + \frac{m_z x}{I_{zz}} \tag{24}$$

where f_r is the 3/rev radial shear, m_x is the 3/rev flapping moment and m_z is the 4/rev lagging moment. The variables x and z are the respective distances to each of the six corners (see Fig. 9) from the box beam shear center.

Optimization

Objective Functions: For the particular four-bladed articulated rotor considered, it was found that the 4/rev lagging moment, m_z, is more critical than the 3/rev inplane shear force. Therefore, the 4/rev vertical shear (f_z) and the 4/rev lagging moment (m_z) are used as objective functions.

Design Variables: Both aerodynamic and structural design variables are used. Following, is a description of the design variables used.

(i) Chord distribution parameters; c_r, $\tilde{\lambda}$, α and p

(ii) Twist distribution parameters; θ_r, τ and δ

(iii) Box beam wall thicknesses at the root; t_{i_r}; i = 1,2, ... , NMEM

(iv) Nonstructural weights; w_{t_j} and w_{c_j}; j = 1, 2, ... , NSEG

Dynamic Criteria: To avoid any degradation of the remaining vibratory loads, not selected as objective functions, upper bound constraints are imposed on these forces and

moments. In the previous problem[24], "windows" were placed on the blade natural frequencies to avoid resonance. However, it was determined that these constraints are included implicitly through the constraints on the vibratory loads. Therefore, in this problem, the frequency constraints are deleted from the constraint vector. The dynamic constraints are summarized below.

(i) 3/rev radial shear; $f_r \leq f_{rU}$

(ii) 3/rev inplane shear; $f_x \leq f_{xU}$

(iii) 4/rev flapping moments; $m_x \leq m_{xU}$

(iv) 4/rev torsional moments; $m_c \leq m_{cU}$

Aerodynamic Criteria: The rotor power required is a measure of economic efficiency. Therefore, it is important to ensure that the power required for the optimum blade is no greater than the reference blade. This constraint is imposed by placing an upper bound on the total power coefficient C_P. A lower bound is also imposed on the total rotor thrust to satisfy the thrust carrying capability of the rotor. These constraints are formulated as follows.

(v) $C_P \leq C_{PU}$

(vi) $T \geq T_L$

Structural Criteria: The problem was formulated to include upper bound constraints on the total stress at each blade segment. However, during initial stages of the optimization, it was found that these constraints were never critical. Therefore, they are eliminated from the final optimization constraint vector. The stresses are however monitored throughout the optimization process to ensure that they are well below the allowable levels. The structural constraints are summarized below.

(vii) $W \leq W_U$

(viii) $AI \geq AI_L$

where W is the total blade weight and AI is the autorotational inertia.

Aeroelastic Criteria: Since an articulated rotor is used as a baseline design, a simple constraint on the offset between the shear center and the center of mass of the blade, x_e, can prevent classical bending-torsion flutter. In order to ensure that the optimized blade is aeroelastically stable, a constraint is imposed on this shear center offset as follows.

(ix) $x_{e_i} \geq 0; \quad i = 1, 2, \ldots, NSEG$

This ensures that the center of mass is always located forward of the shear center throughout the blade span.

Analysis

Dynamic, Aerodynamic and Aeroelastic Analyses: The program CAMRAD is used for both blade dynamic and aerodynamic analyses. The rotor is trimmed, as before, using a wind tunnel trim option. However, in the previous problem, the rotor was trimmed to a C_T/σ value equal to that of the reference rotor during optimization. This, coupled with the constraint on the total thrust coefficient, C_T, fixed the solidity of the optimum rotor to that of the reference (σ_{ref}) rotor. To avoid this indirect constraint on the solidity, the following trim procedure is implemented in this problem.

$$(C_T/\sigma)_{trim} = (C_T/\sigma)_{ref} \times (\sigma_{ref}/\sigma) \tag{25}$$

where σ denotes the current value of the solidity corresponding to the particular cycle. This allows for the optimum blade to be trimmed to a different value of C_T/σ at each cycle.

Structural Analysis: The detailed structural analysis of the rotor blade is performed using an inhouse code that was recently developed specifically for these applications. The code models a simple two cell homogeneous box beam with one rectangular cell and one trapezoidal cell (Fig. 9). The structural properties are calculated using the thin wall theory[54] and the assumption of a homogeneous isotropic material. The beam is symmetric

about the x-axis and is assumed to be the sole load-carrying member within the rotor. It is also assumed that the flatwise, chordwise and torsional stiffnesses of the blade are provided only by the box beam.

Optimization Implementation

The optimization problem is formulated using the Min $\Sigma\beta$ and the K-S function approaches as discussed earlier. The same optimization algorithm (CONMIN) is used and the sensitivity analysis is performed using forward finite difference. A first order linear Taylor series-based approximation procedure is used for the approximate analysis (discussed in detail in Chapter III).

Results and Discussions

A wind tunnel model of the Growth Black Hack rotor blade (R = 4.685 ft., Ω = 639.5 RPM) is used as the reference design. Optimization is performed in the forward flight condition with an advance ratio, μ = 0.3. For this problem, the rotor blade is discretized into 10 segments (NSEG = 10) and the value of five wall thicknesses of the box beam are used as independent design variables, i.e. NMEM = 5 (see Fig. 9). The total number of design variables used is 32 for the K-S function approach and 34 for the Min $\Sigma\beta$ approach, which includes the two pseudo design variables β_1 and β_2.

The optimum results are summarized in Tables 3 and 4 and Figs. 13 - 20. Table 3 presents a summary of the important results. Substantial reductions are obtained in the objective function values. The 4/rev vertical shear (f_z) is reduced by 17.6 percent in the K-S function approach and by 14.9 percent in the Min $\Sigma\beta$ approach. The 4/rev lagging moment (m_z) is reduced by 4.4 and 2.1 percent for Min $\Sigma\beta$ and K-S function approaches, respectively (Table 3). The constraints are all satisfied in both cases. It is important to note that the coefficient of total power (C_P) is reduced by 4.3 percent in both cases. This represents a significant increase in the economic efficiency in the optimum rotor. The

thrust (T) is slightly increased (less than 1 percent) in the K-S function approach and is at the prescribed lower bound in the Min $\Sigma\beta$ approach thus guaranteeing equivalent lifting capability as the reference rotor. The situation is reversed for the autorotational inertia (AI), with the Min $\Sigma\beta$ case yielding a slight increase (less than 1 percent) and the constraint being critical in the K-S function case. For the Min $\Sigma\beta$ case, the 3/rev radial shear (f_r), the 3/rev inplane shear (f_x) and the 3/rev flapping moment (m_x) are all reduced by nearly 4 percent and the 3/rev torsional moment, m_c, is critical. In the K-S function approach, f_x is held at its upper bound, and f_r and m_x are reduced by 5.6 and 5.4 percent, respectively. The 3/rev vibratory torsional moment (m_c) is reduced by 2.9 percent in the K-S function case and is equal to the reference blade value in the Min $\Sigma\beta$ approach. The total weight (W) is also slightly reduced in both cases (less than 1 percent in the Min $\Sigma\beta$ case and 1.4 percent in the K-S function case). It is interesting to note from Table 3, that the solidity, σ, of both the optimum rotors is close to the reference rotor (very marginal decrease) although the solidity was allowed to vary during optimization. Therefore, the value of C_T/σ for both the optimum and reference rotors remains almost the same (the optimum rotors have a slightly higher value) indicating that the rotor aerodynamic efficiency is maintained after optimization. Figure 13 more clearly depicts the significant reductions in the normalized objective functions, f_z and m_z, and the total power coefficient, C_P. The large reductions in C_P can be attributed to the inclusion of aerodynamic design variables.

Table 4 and Figs 15 and 16 present the design variables, before and after optimization. Table 4 shows that in both cases the optimum blade has a larger root chord, c_r, and is slightly tapered ($\tilde{\lambda} = 0.96$ and 0.94 for the Min $\Sigma\beta$ and K-S function cases, respectively). The chord shape parameters α and p are nearly equal to the reference values in the Min $\Sigma\beta$ approach, whereas in the K-S function approach, α experiences a 14 percent increase and *p reduces by 12 percent.* In the Min $\Sigma\beta$ approach, the root twist, θ_r, is reduced by 1.7 percent and the twist ratio, τ, is increased by 7.8 percent (from reference blade) and the

twist distribution is nearly linear with a shape parameter $\delta = 0.957$ (see Fig. 12). As indicated in Table 4, the K-S function approach produces very similar results, however in this case θ_r is increased by 1.5 percent and τ is reduced by 5.7 percent. The twist distribution is again very nearly linear with $\delta = 0.963$ (Fig. 12). The box beam wall thicknesses demonstrate significantly different trends for the two cases. In the Min $\Sigma\beta$ approach, the thicknesses are increased for the upper and lower walls (t_4) and (t_5) by 4.2 percent and 6.1 percent respectively. In the K-S function case t_4 is reduced by 6.6 percent and t_5 experiences a substantial reduction of 23.4 percent. Similarly, the vertical member nearest to the leading edge, t_1, is decreased by 2.9 percent using the Min $\Sigma\beta$ approach and is increased by 2.3 percent using the K-S function approach. The centrally located vertical member, t_2, is marginally reduced in the Min $\Sigma\beta$ approach (less than 1.0 percent) and is increased slightly (2.0 percent) in the K-S function approach. The thickness, t_3, of the aft vertical member is increased in both cases, although more dramatically in K-S function case (11.8 percent). Overall, the stiffness of the optimum blade in the K-S function case is greater than the optimum blade in the Min $\Sigma\beta$ case. This indicates convergence to significantly different local minima in the two cases. The root stiffnesses of both of the optimum blades are greater than the reference blade as indicated in Fig. 14.

Table 3 Summary of Integrated Helicopter Rotor Blade Optimization Results

	Reference blade	Bounds lower	Bounds upper	Optimum Min $\Sigma\beta$	Optimum K-S
Objective Functions					
4/rev f_Z (lb)	0.201	-	-	0.171	0.166
4/rev m_Z (lb -ft)	1.43	-	-	1.37	1.40
Constraints					
AI (lb-ft^2)	18.4	18.4	-	18.5	18.4
W (lb)	3.18	-	3.18	3.17	3.13
3/rev f_r (lb)	0.515	-	0.515	0.496	0.486
3/rev f_X (lb)	0.331	-	0.331	0.325	0.331
3/rev m_C (lb -ft)	0.119	-	0.119	0.119	0.116
3/rev m_X (lb -ft)	1.12	-	1.12	1.07	1.06
T (lb)	282	282	-	282	283
C_p	0.00105	-	0.00105	0.00100	0.00100
x_{e_1}	0.0137	0.0	-	0.0138	0.0182
x_{e_2}	0.0137	0.0	-	0.0149	0.0136
x_{e_3}	0.0137	0.0	-	0.0143	0.0143
x_{e_4}	0.0137	0.0	-	0.0151	0.0144
x_{e_5}	0.0137	0.0	-	0.0159	0.0159
β_1	0.100	0.005	0.105	0.058	-
β_2	0.100	0.005	0.105	0.056	-
Solidity σ	0.116	-	-	0.115	0.114
Trim C_T/σ	0.0591	-	-	0.0593	0.0592

Table 4 Summary of Integrated Helicopter Rotor Blade Optimization Design Variables

	Design Variables	Reference	Optimum	
			Min $\Sigma\beta$	K-S
wall thickness at the root	t_{r_1} (in)	0.0312	0.0303	0.0319
	t_{r_2} (in)	0.0312	0.0311	0.0320
	t_{r_3} (in)	0.0312	0.0316	0.0349
	t_{r_4} (in)	0.0312	0.0325	0.0292
	t_{r_5} (in)	0.0312	0.0331	0.0386
root chord	c_r (ft)	0.450	0.458	0.462
chord shape parameters	$\tilde{\lambda}$	1.00	0.956	0.943
	α	0.0100	0.0101	0.0114
	p	0.0100	0.00984	0.00882
root twist	θ_r (deg)	30.0	29.5	30.4
twist shape parameters	τ	- 0.333	- 0.359	- 0.314
	δ	1.00	0.957	0.963

Figure 15 presents comparisons of the nonstructural weight distributions w_t (located at the leading edge) and w_c (located at 35 percent chord). Using both multiobjective formulation procedures, similar trends are obtained in the w_t and w_c distributions. All of these distributions display reductions at inboard locations and increases towards blade outboard. However, the changes are more significant in the K-S function approach, particularly in the case of w_c. The trend can be explained as follows. In an effort to satisfy the autorotational inertia constraint in addition to the constraint on the blade weight, the optimizer redistributes the weight such that the overall weight decreases whereas the outboard weights, which have larger effects on the blade autorotational inertia, increase. The large increases in the outboard nonstructural weights in the K-S function approach allow for similarly large decreases at blade inboard. This leads to a greater overall reduction in weight, as indicated in Table 3.

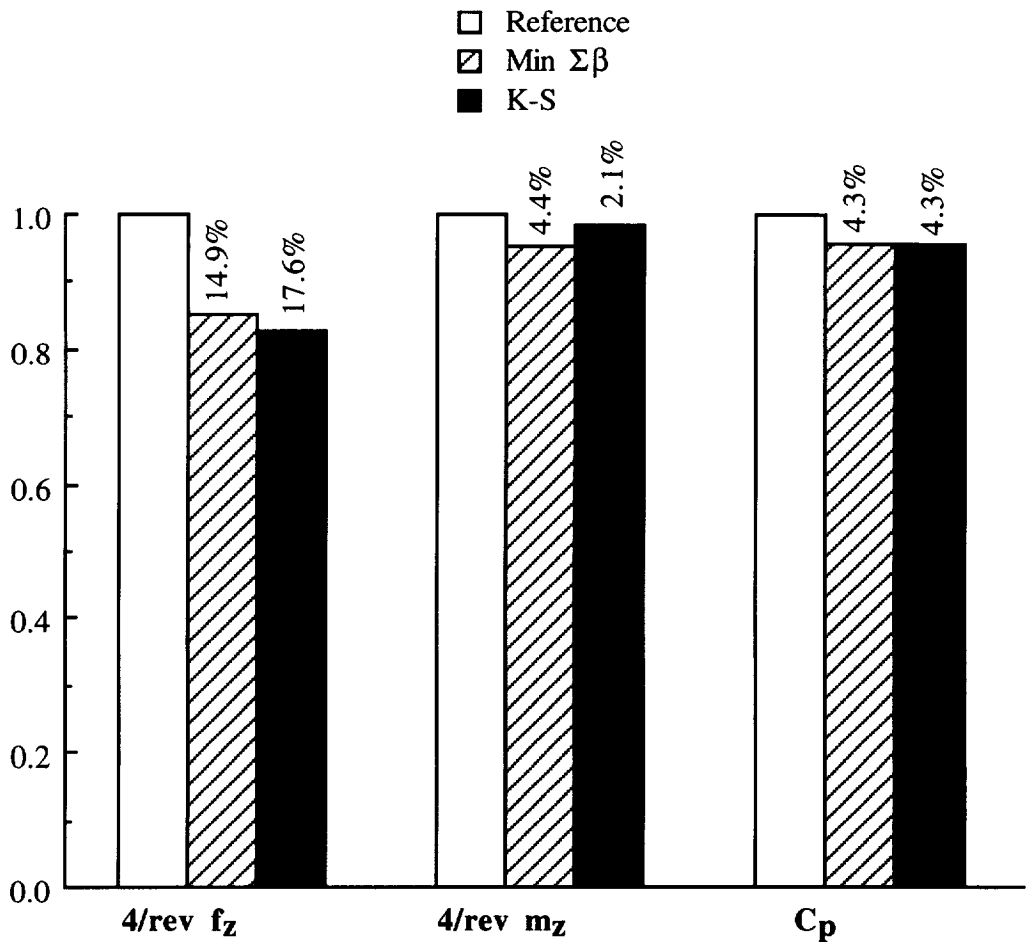

Figure 13 Comparisons of normalized vibratory loads and total power

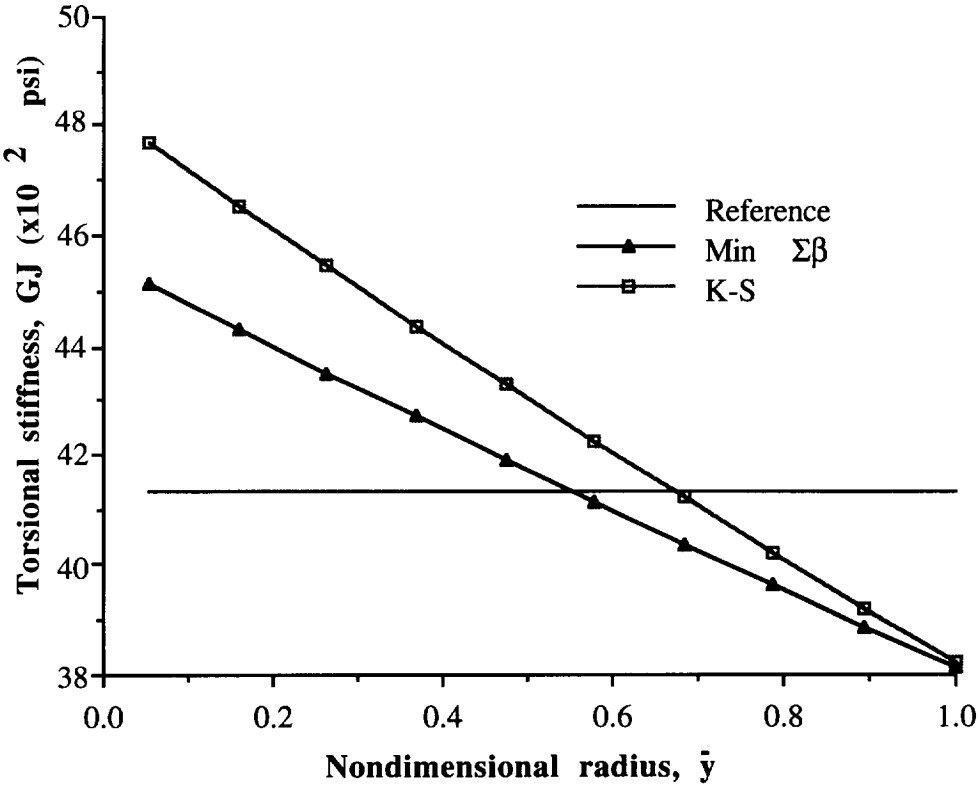

Figure 14 Blade stiffness distribution

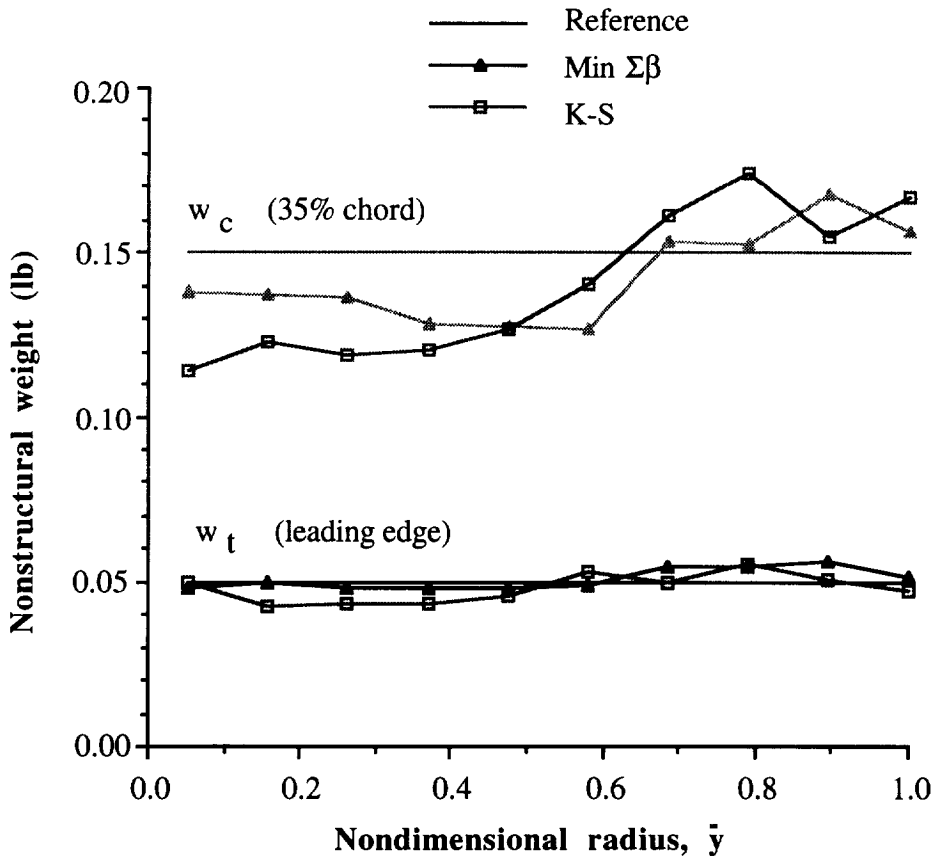

Figure 15 Blade nonstructural weight distributions

The chord distributions of the reference and the optimum rotors are presented in Figure 16. This figure shows that the optimum blades, in both cases have slightly increased root chords and slightly tapered planforms. As indicated in the figure, the chord values at the tip are nearly identical to the reference blade despite the fact that in the K-S function approach there are significant changes in the tip shape parameters. This indicates that the root chord and taper ratio have more control on the blade planform than the tip shape parameters, α and p.

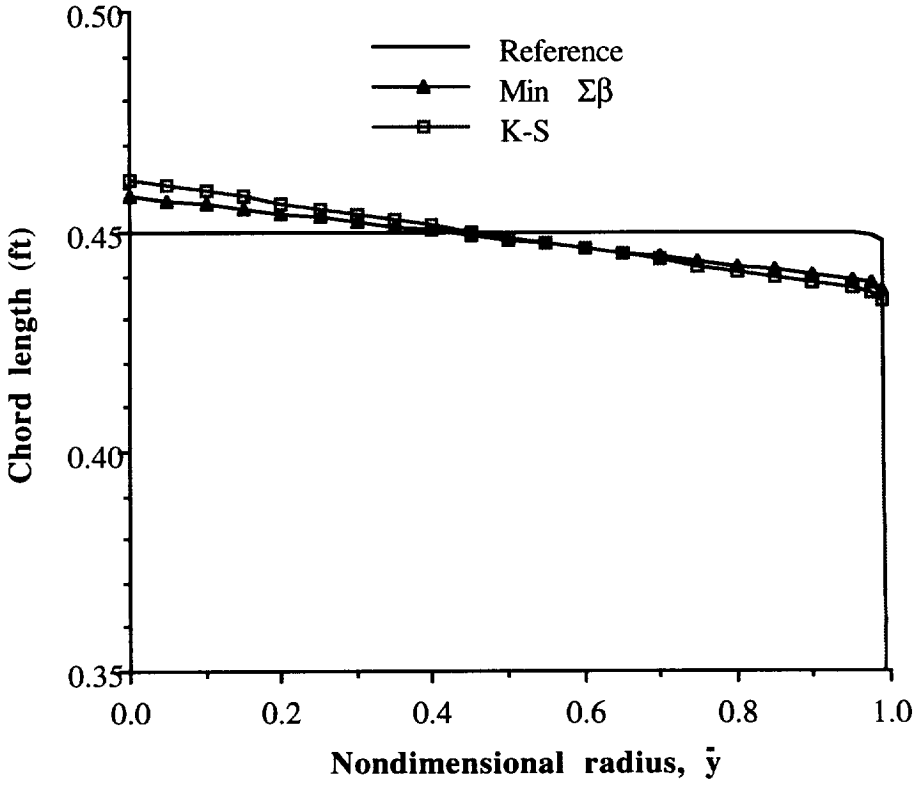

Figure 16 Chord distribution

Figure 17 presents the spanwise distribution of the center of gravity offset from the elastic axis, x_e. The figure illustrates satisfactory values of x_e throughout the blade span in both cases. The center of gravity offsets are directly related to the distributions of the nonstructural weights. In the Min $\Sigma\beta$ approach, the reductions in w_c are greater than the reductions in w_t at inboard and mid span locations which shifts the center of gravity forward thereby increasing x_e. At the tip where changes in the nonstructural weights have less effect (due to the smaller chord length), the increase in w_c is greater than the increase in w_t. This tends to shift the center of gravity aftward and reduces x_e. In the K-S function case, the changes in w_c are much greater than the corresponding changes in w_t and x_e is therefore primarily driven by w_c. As indicated in Figs. 15 and 17, reductions in w_c lead to

increased values of x_e and vice versa except at a few inboard locations. At these locations, reductions in w_t (from reference values) are large and x_e remains close to the reference.

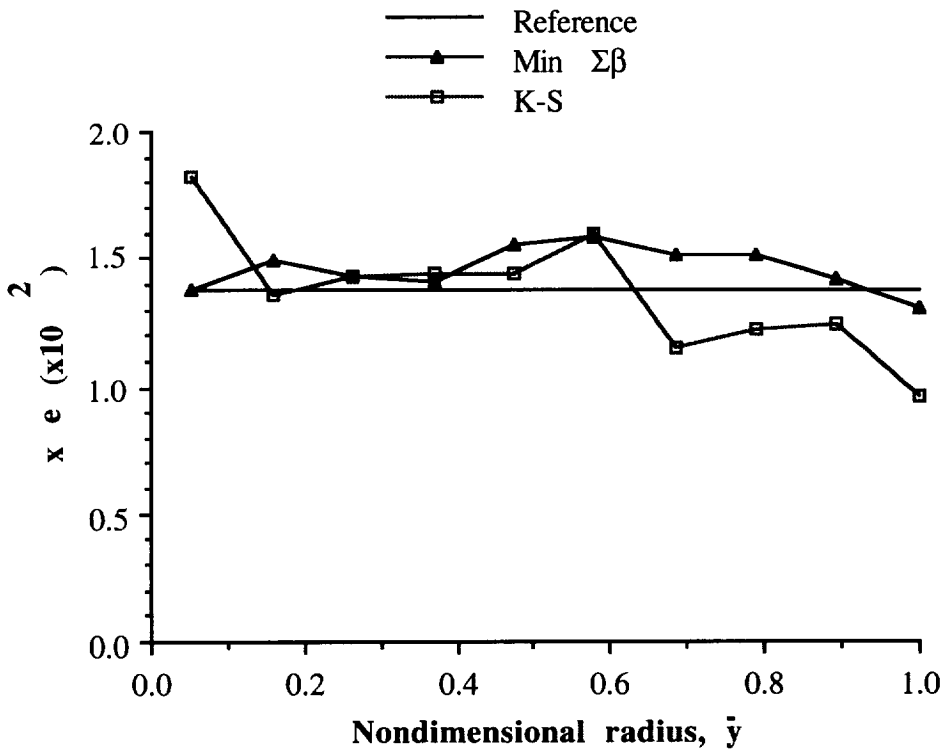

Figure 17 Blade center of gravity offset distribution

Figure 18 displays the convergence history of the individual objective function, 4/rev vertical shear (f_z) and demonstrates substantial increases using both multiobjective formulation approaches. The objective function oscillates before converging to the final solution. Similar observations are made on the 4/rev lagging moment, m_z (Fig. 19). The oscillatory behavior is attributed to the highly nonlinear nature of the objective functions and the use of the approximate analysis technique (first order linear Taylor series expansion).

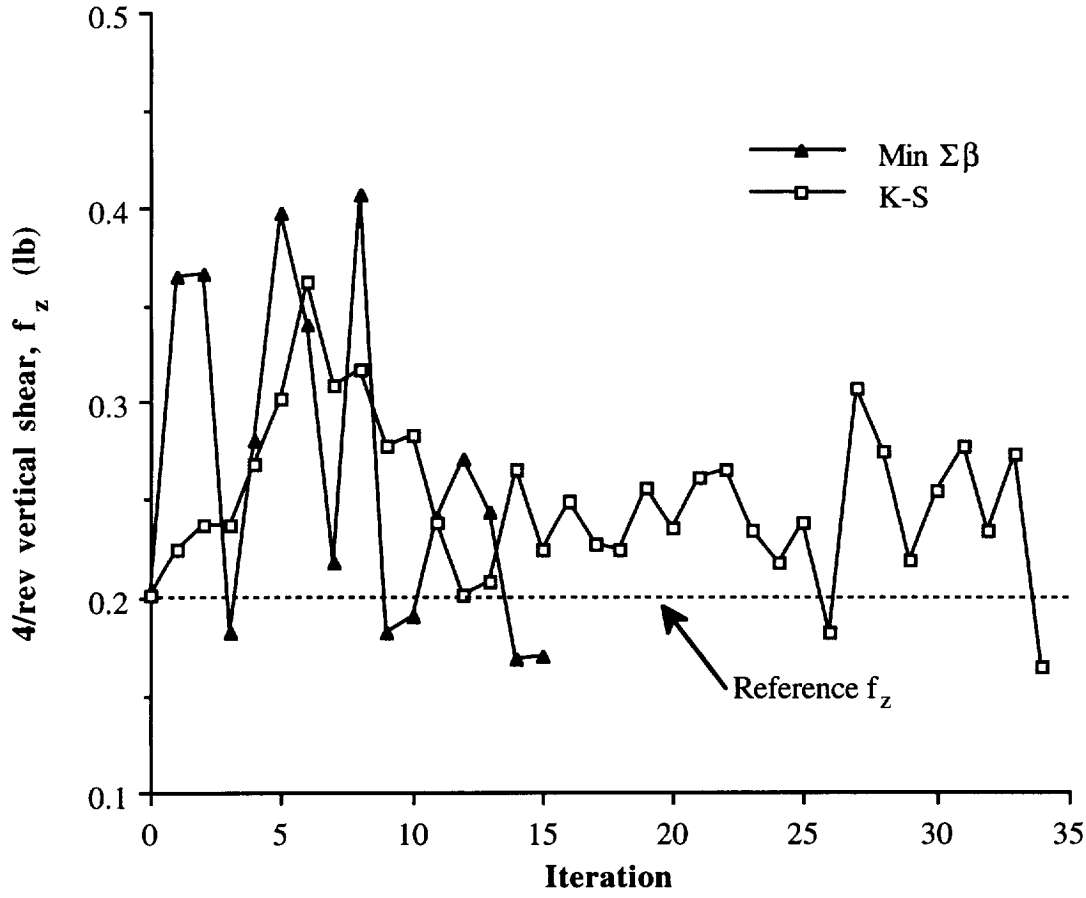

Figure 18 4/rev vertical shear iteration history

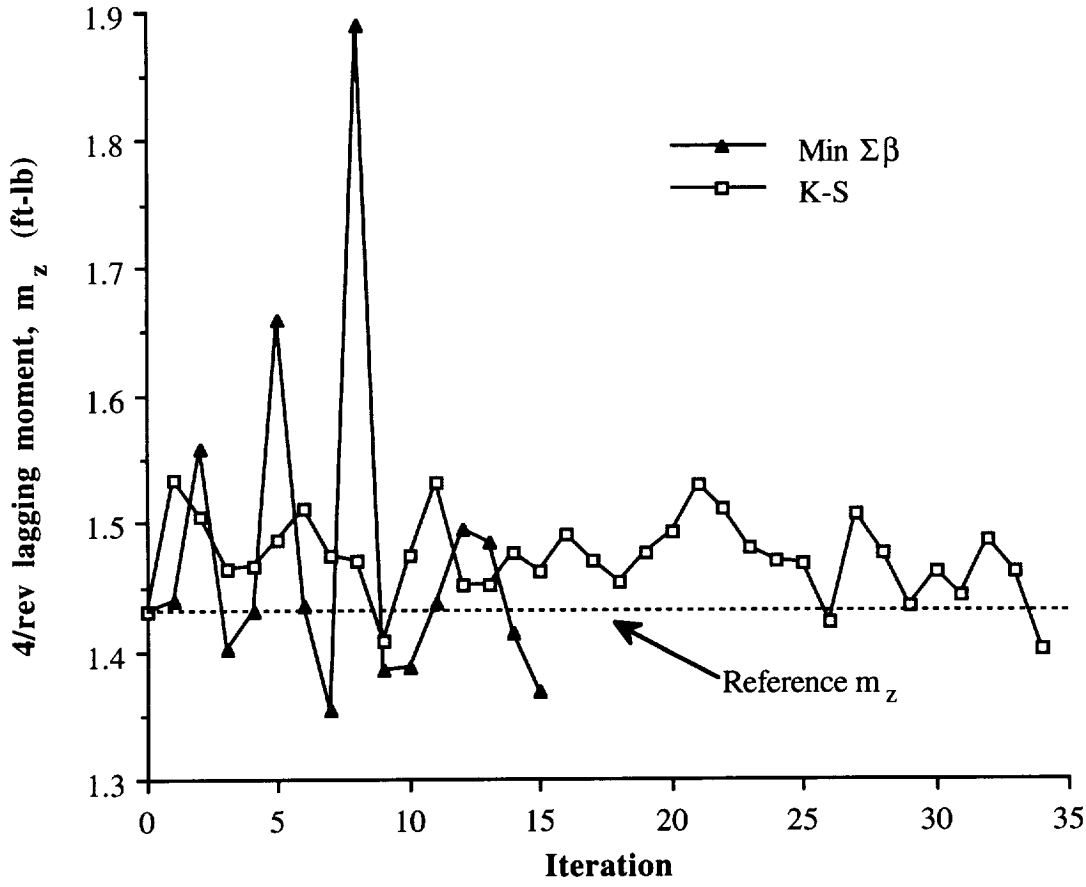

Figure 19 4/rev lagging moment iteration history

Figure 20 displays the convergence history of the compound objective functions used in the Min $\Sigma\beta$ and K-S function cases. The figure indicates a smooth convergence, that is achieved in 15 cycles, in the Min $\Sigma\beta$ approach. This is expected since the objective function is strictly linear ($F(\Phi) = \beta_1 + \beta_2$). However, in the K-S function approach, the objective function is highly oscillatory. This can be explained by noting that the value of the K-S function (Eqn. 6) is driven primarily by the largest violated constraint, f_{max}, which for this problem corresponds to g_{max}. Therefore in an attempt to reduce the objective function, the optimizer tries to satisfy this constraint more vigorously than the others. This in turn, in the next cycle, produces a new constraint as the maximum violated constraint (g_{max}) which due to the nonlinearities of the rotor blade problem is often violated to same

degree as the previous g_{max} had been. Therefore the objective function is discontinuous from one cycle to the next.

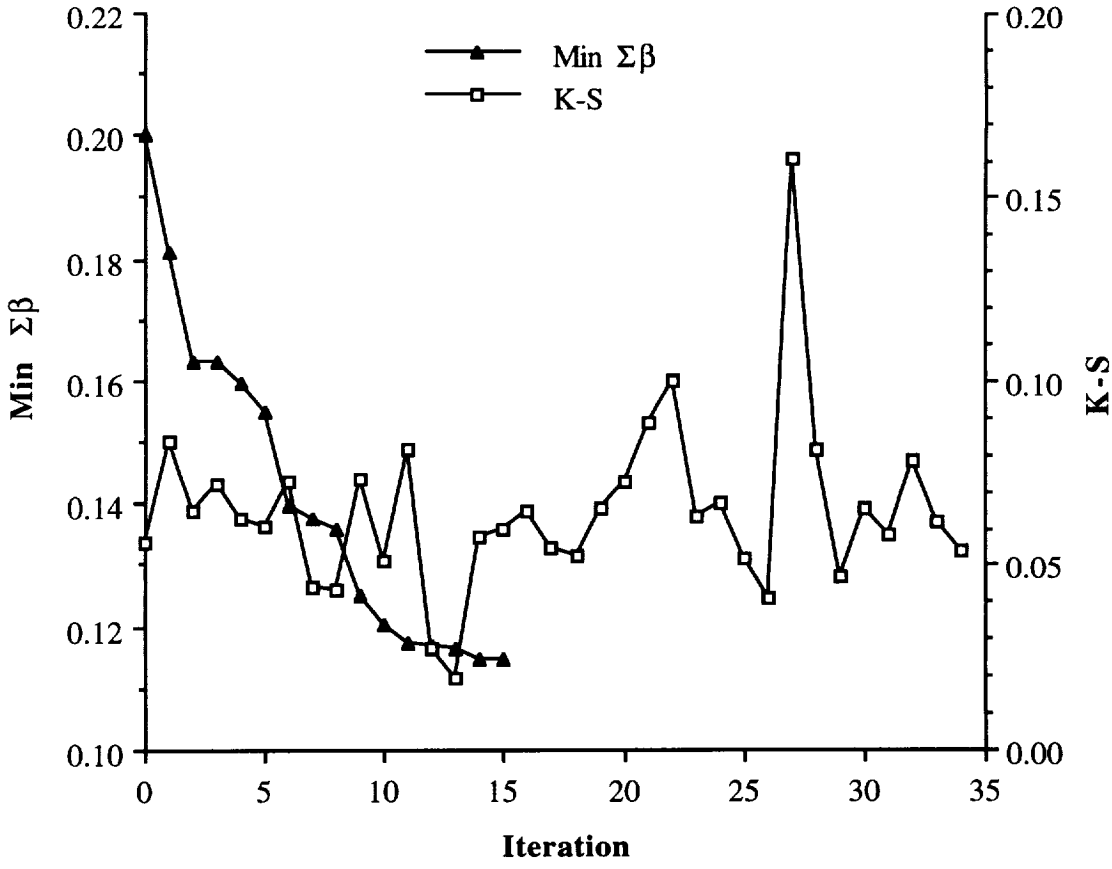

Figure 20 Objective function convergence history

Conclusions

This problem addresses the coupling of rotor dynamic, aerodynamic, structural and aeroelastic issues within a closed-loop optimization procedure. Blade root 4/rev vertical shear and 4/rev lagging moments are reduced with constraints imposed on the remaining critical vibratory forces and moments, rotor thrust, total power coefficient, autorotational inertia, blade weight and the center of gravity - elastic axis offset. A two-celled box beam is designed as the principal load-carrying member inside the airfoil. Design variables

include wall thicknesses of the box beam, magnitudes of the nonstructural weights located at the leading edge and at 35 percent chord (inside the box beam), chord and twist distributions. A Minimum Sum Beta (Min $\Sigma\beta$) and a Kreisselmeier - Steinhauser (K-S) function approach are used to formulate the multiobjective design problem. An existing blade model is used as a reference or baseline design. Optimum designs, obtained using both cases, are compared to the reference design. The following important observations are made.

1) Significant reductions were obtained in both the objective functions (4/rev vertical shear, 14.9 and 17.6 percent, and lagging moment, 4.4 and 2.1 percent, respectively for the Min $\Sigma\beta$ and K-S function cases). The remaining constraints were well satisfied.
2) Results obtained indicated convergence to two different local optimum points.
3) The nonstructural weights, located at both leading edge and at 35 percent chord locations, demonstrated similar trends of reductions at blade inboard locations and increases towards outboard. This was the result of the weight and the autorotational inertia constraint which are conflicting in nature.
4) The optimum chord distributions were tapered and the twist distributions were almost linear for both optimization formulation approaches.
5) The influence of the aerodynamic design variables (twist in particular) was demonstrated through the significant reductions in the total power coefficient (C_P) which was reduced significantly (4.4 percent for both the Min $\Sigma\beta$ and the K-S function approaches).

V. Integrated High-Speed Proprotor Optimization

Problem Definition

A multidisciplinary, multiobjective optimization procedure is developed for the design of high-speed proprotors. The objectives are to maximize propulsive efficiency in high-speed cruise without sacrificing rotor figure of merit in hover. Constraints are imposed on rotor blade aeroelastic stability in cruise and on total blade weight. The Min $\Sigma\beta$ and the K-S function approaches are used to formulate the two-objective optimization problem.

Blade Model

The rotor used for the integrated high-speed proprotor optimization is a wind tunnel model of the XV-15 proprotor[40], which is a three bladed rotor with a rigid hub. The load carrying structural member is modeled using a two-celled box beam as used in the helicopter rotor blade optimization problem described in Chapter IV. One difference, however, is that the only nonstructural weights used in this problem are those that are located at the leading edge of the airfoil [Fig. 9]. Also, the weights for the blade skin and honeycomb components are estimated and included in the calculations for the blade total weight and the center of gravity. The total nonstructural weight is calculated as follows.

$$W_{ns_i} = L_i\left[\left(\frac{w_{t_i} + w_{t_{i+1}}}{2}\right)+\left(\frac{w_{hc_i} + w_{hc_{i+1}}}{2}\right)+\left(\frac{w_{sk_i} + w_{sk_{i+1}}}{2}\right)\right] \tag{26}$$

where w_{t_i} is the nonstructural weight per unit length at the leading edge of the airfoil and w_{sk_i} and w_{hc_i} represent the weight per unit length of the blade skin and honeycomb, respectively. It is important to note that although the structural model used is the same as in the helicopter rotor blade optimization problem, the geometric parameters such as the angle of the trapezoid and the outer dimensions of the beam are different in the two problems since they depend upon the airfoil shape.

Cubic variations are assumed for the chord and twist distributions to model the blade aerodynamics,

$$c(\bar{y}) = c_o + c_1(\bar{y} - 0.75) + c_2(\bar{y} - 0.75)^2 + c_3(\bar{y} - 0.75)^3 \tag{27}$$

$$\theta(\bar{y}) = \theta_o + \theta_1(\bar{y} - 0.75) + \theta_2(\bar{y} - 0.75)^2 + \theta_3(\bar{y} - 0.75)^3 \tag{28}$$

Note that, in the above equations, c_o represents the chord and θ_o the twist at the 75 percent radius, respectively. A quadratic lifting line is used and is defined as follows.

$$x = f(y) = \varepsilon_1 y + \varepsilon_2 y^2 \tag{29}$$

where ε_1, ε_2 are constants that determine the curvature, and are defined such that

$$| \varepsilon_i | \leq \zeta_i \tag{30}$$

where ζ_i is a prescribed bound for the curvature parameters. These bounds allow for either forward or backward in-plane curvatures. When ε_1 and ε_2 are equal to zero the lifting line will be a straight line. The blade sweep, based upon this lifting line distribution, assumes the following form

$$\Lambda(\bar{y}) = \frac{180}{\pi}\tan^{-1}\left(\frac{dx}{dy}\right)$$

$$= \frac{180}{\pi}\tan^{-1}(\varepsilon_1 + 2\varepsilon_2\bar{y}) \tag{31}$$

where $\bar{y}$ is the nondimensional radial location and $\Lambda(\bar{y})$ is the sweep distribution, in degrees, defined to be positive aft of the straight lifting line.

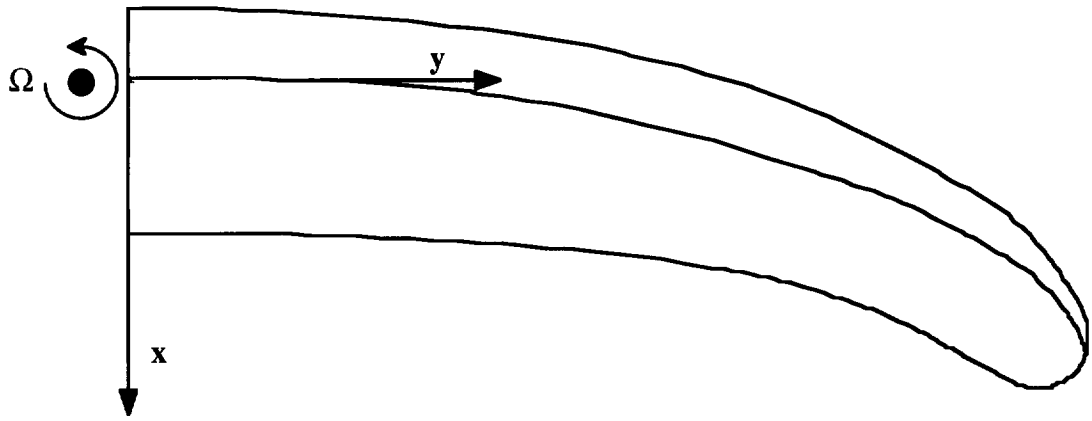

Figure 21 Swept blade planform

Optimization

Objective Functions: The multiobjective optimization procedure is used to simultaneously maximize the rotor propulsive efficiency, η_{ax}, at high-speed cruise and the hover figure of merit, FOM.

Design Variables: Both aerodynamic and structural design variables are used. The aerodynamic design variables include chord, twist and sweep distributions. The structural design variables comprise root values of the thicknesses of the several walls of the two-cell box beam and magnitudes of the nonstructural weights distributed spanwise. These design variables are summarized as below.

(i) Chord distribution coefficients; c_o - c_3

(ii) Twist distribution coefficients; θ_o - θ_3

(iii) Sweep parameters; ε_1 and ε_2

(iv) Box beam wall thicknesses at the root; t_{i_r}; i = 1 and 4

(v) Nonstructural weights at the leading edge; w_{t_j}; j = 1, 2, ... , NSEG

Dynamic Criteria: To avoid the possible occurrences of air and/or ground resonance, associated with a soft inplane rotor, it is important to maintain the value of the lowest natural frequency in hover (f_1) above 1/rev. Therefore the following constraint is imposed.

(i) $f_1 > 1/\text{rev}$

Aeroelastic Criteria: It is important to impose aeroelastic stability constraints to prevent any degradation of the rotor stability in high-speed cruise. This is all the more important when the blade mass and stiffness are altered during optimization. The stability constraints are expressed as follows.

(ii) $\alpha_k \leq -\upsilon_k \qquad k = 1, 2, \ldots, K$

where K represents the total number of modes considered and α_k is the real part of the stability root. The quantity υ_k denotes the minimum allowable blade damping and is defined to be a small positive number.

Structural Criteria: to avoid incorporation of weight penalties, after optimization, the total blade weight is constrained as follows.

(iv) $W \leq W_U$

As in the case of the helicopter rotor blade problem, it was found that the rotor centrifugal stresses remain well below the critical values. Therefore, they are not included in the constraint vector, but are monitored during the optimization procedure.

Analysis

Dynamic, Aerodynamic and Aeroelastic Analyses: The aerodynamic, dynamic and aeroelastic analysis of the high-speed proprotor is performed using the code CAMRAD/JA[34]. The code has the capability of analyzing both helicopter and tilting rotor aircraft. Once again, wind tunnel trim options are used since the reference blade is a wind tunnel model. In cruise, the blade is trimmed to specific rotor lift and drag coefficients

using the rotor collective and cyclic pitch angles. A prescribed wake model, as implemented in CAMRAD/JA, is used to model the aerodynamics in hover and the rotor is trimmed to a specific value of the coefficient of power. However, in axial flight, the components of the induced velocity are negligible compared to the high forward speed of the rotor. Therefore, uniform inflow conditions are used to model the aerodynamics in this case. The aeroelastic stability analysis for the cruise case are analyzed with assumption of a constant coefficient state model. Three bending degrees of freedom and one torsional degree of freedom are used.

Structural Analysis: The two-celled box beam section is analyzed using thin wall theory as before (Chapter IV).

Optimization Implementation

The optimization algorithm and the sensitivity analysis procedure are identical to those described in Chapter III. However, a hybrid technique is used to improve the approximation method since the problem is highly nonlinear and as noted in the previous cases of helicopter optimizations, very small move limits were necessary to justify the assumption of linearity imposed by the first order linear Taylor series expansion. To overcome this, a two-point exponential approximation[55] is used in this problem. The technique takes its name from the fact that the exponent used in the expansion is based upon gradient information from the previous design point and is formulated as follows.

$$\hat{F}(\Phi) = F(\Phi_o) + \sum_{n=1}^{NDV}\left[\left(\frac{\phi_n}{\phi_{o_n}}\right)^{p_n} - 1.0\right]\frac{\phi_{o_n}}{p_n}\frac{\partial F(\Phi_o)}{\partial \phi_n} \tag{32}$$

where

$$p_n = \frac{\log\left\{\left(\frac{\partial F(\Phi_1)}{\partial \phi_n}\right) \Big/ \left(\frac{\partial F(\Phi_o)}{\partial \phi_n}\right)\right\}}{\log\left(\frac{\partial \phi_{1_n}}{\partial \phi_{o_n}}\right)} + 1.0 \qquad (33)$$

The quantity Φ_1 refers to the design variable vector from the previous iteration and the quantity Φ_0 denotes the current design vector. A similar expression is obtained for the constraint vector. The exponent p_n can be considered as a "goodness of fit" parameter, which explicitly determines the trade-offs between traditional and reciprocal Taylor series based expansions (also known as a hybrid approximation technique). It can be seen from Eqn. 33 that in the limiting case of $p_n = 1$, the expansion is identical to the traditional first order Taylor series and with $p_n = -1$ the two-point exponential approximation assumes the reciprocal expansion form. The exponent is therefore defined to lie within this interval, such that if $p_n > 1$, it is set identically equal to one, and if $p_n < -1$, it is set equal to -1. From Eqns. 32 and 33, it is obvious that singularities can arise while using this method, therefore, care must be taken to avoid such points. When such singular points do arise, the approximation method used is the linear first order Taylor series based method.

Results and Discussions

A wind tunnel model of an existing high-speed proprotor is used as a baseline design. The optimization for this problem is performed with a cruise velocity of 400 knots and a rotational velocity of $\Omega = 375$ RPM (tip speed of 491 ft/s) in axial flight. The operating condition is 20,000 feet above sea level. In hover, a rotational velocity of $\Omega = 570$ RPM (tip speed of 746 ft/s) is used at sea-level conditions. The high forward flight speed of 400 knots represents the target cruise value for high-speed rotorcraft. The rotor RPM in cruise is selected after performing a parametric study on the effect of forward speed and rotor

RPM on propulsive efficiency. A value of $C_T/\sigma = 0.08$ is used to trim the blade in forward flight and a value of $C_p/\sigma = 0.0131$ is used to trim the blade in hover. The blade radius is 12.5 feet, and the blade is discretized into 10 segments (NSEG = 10). In the K-S function approach 22 design variables are used and, including the pseudo-design variables, 24 design variables are used in the Min $\Sigma\beta$ approach.

The optimum results for this problem are summarized in Tables 5 and 6 and Figs. 22 - 32. From Table 5 and Fig. 22 it can be seen that there are substantial increases in both the hover figure of merit (FOM) and the axial propulsive efficiency (η_{ax}) using both multiobjective formulation techniques. A 21.7 percent increase in η_{ax} and a 28.8 percent increase in FOM are obtained in the Min $\Sigma\beta$ approach. More significant improvements are obtained using the K-S function approach which yields a 24.6 percent increase in η_{ax} and a 41.3 percent increase in FOM. The constraints in both cases are all well satisfied, most notably in the K-S function case, where the constraints are far from their respective limits. In the Min $\Sigma\beta$ case, the first natural frequency in hover (f_1) is the driver constraint, as it remains active or nearly active throughout the optimization. It is of interest to note that the mean chord (and correspondingly the blade solidity) is increased by 71 percent and 40 percent in the K-S function and Min $\Sigma\beta$ approaches, respectively from the baseline value. Two possible explanations exist for the large increases in the rotor solidity. First, in order to satisfy the frequency constraint, the root chord is significantly increased to make the stiffnesses larger, which in turn increases the solidity. Secondly, since FOM is being maximized, σ is being increased to increase the thrust margin of the rotor in hover.

Table 5 Summary of Integrated High-Speed Proprotor Optimization Results

	Reference blade	Bounds lower	Bounds upper	Optimum Min $\Sigma\beta$	Optimum K-S
Objective Functions					
FOM	0.662	-	-	0.853	0.936
η_{ax}	0.647	-	-	0.787	0.805
Constraints					
W (lb)	194	-	194	167	173
f_1 (per rev)	0.812	1.00	-	1.01	1.34
α_1	0.096	-	-0.001	-0.040	-1.529
α_2	0.096	-	-0.001	-0.040	-1.529
α_3	-0.697	-	-0.001	-0.732	-0.169
α_4	-0.697	-	-0.001	-0.732	-0.169
α_5	-2.431	-	-0.001	-2.443	-2.502
α_6	-0.170	-	-0.001	-0.265	-0.073
β_1	0.150	0.001	0.200	0.006	-
β_2	0.150	0.001	0.200	0.010	-
Mean chord c_e (ft)	1.48	-	-	2.07	2.52
Solidity σ	0.113	-	-	0.158	0.193
Trim C_T/σ	0.110	-	-	0.117	0.116

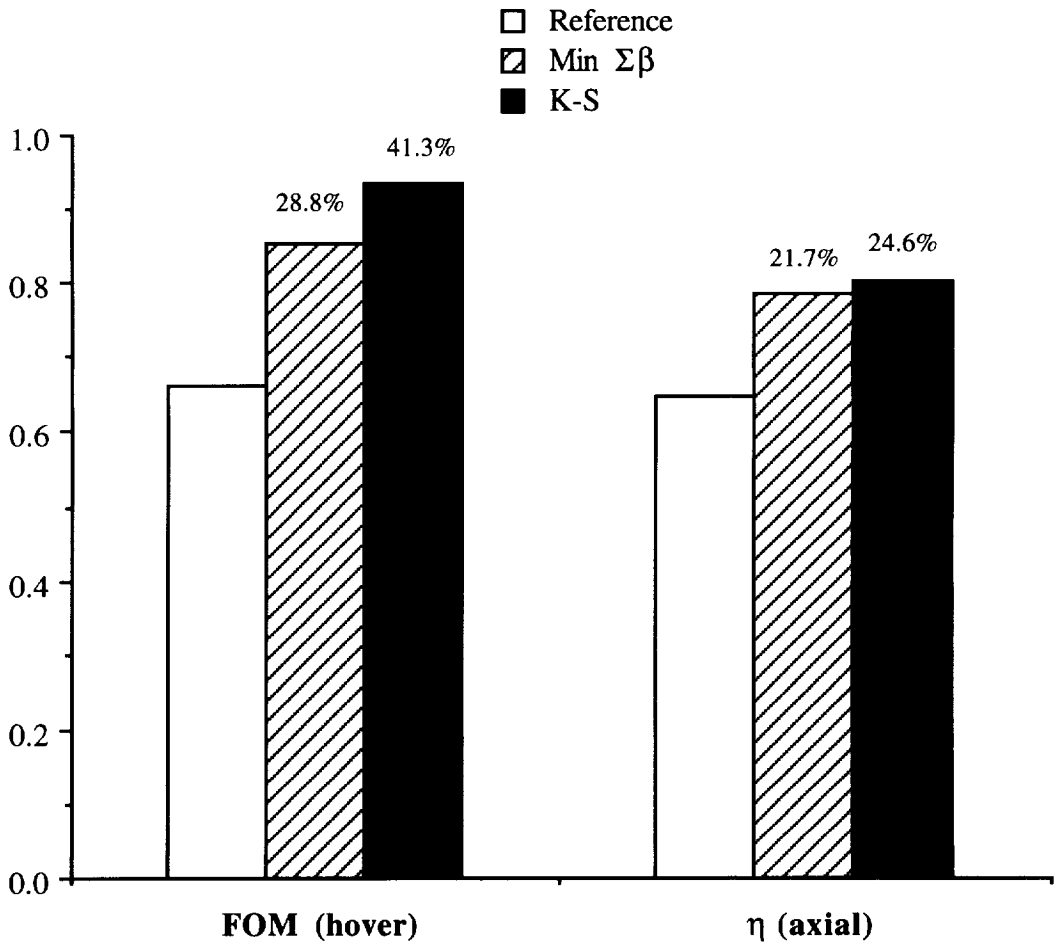

Figure 22 Comparison of individual objective functions

A summary of the design variables is presented in Table 6, Fig. 23 and Figs. 25 - 29. From Table 6 it can be seen that the thicknesses of all the structural elements in both the Min Σβ and K-S function approaches are reduced from the reference values. The largest decrease is in the vertical member in the K-S function approach where there is a 77 percent decrease from the reference value. The thickness of the horizontal member is reduced 25 percent from baseline. In the Min Σβ approach the vertical and horizontal members are reduced by 39 percent and 45 percent, respectively, from the reference values. This trend can be explained by examining the chord distribution (Fig. 23). In an effort to satisfy the rigid-inplane frequency constraint, the optimizer increases the root chord value to increase

the torsional stiffness of the blade, which increases the total blade weight. Therefore, to satisfy both the weight and the frequency constraints, the thicknesses of the structural elements must reduce. Since a larger root chord leads to larger structural eccentricities from the shear center, the stiffnesses are increased while the weight is maintained below the reference value. The stiffness distributions for the optimized and reference blades are shown in Figs. 24 - 26 and show significant increases throughout the blade span, from reference to optimum. The large increase in the root chord in the K-S function approach also explains the subsequently large decreases in the nonstructural weights at locations near the root (Fig. 27). Due to the larger chord values, the effectiveness of the nonstructural weights, at these locations, is magnified since they are further from the elastic axis and therefore have more effect on the center of gravity travel.

Table 6 Summary of Integrated High-Speed Proprotor Optimization Design Variables

	Design Variables	Reference	Optimum	
			Min $\Sigma\beta$	K-S
wall thickness at the root	t_{r_1} (in)	0.400	0.246	0.091
	t_{r_4} (in)	0.400	0.219	0.283
chord shape parameters	c_o	0.121	0.165	0.185
	c_1	-0.152	-0.158	-0.096
	c_2	-0.487	-0.416	-0.213
	c_3	-0.461	-0.372	-0.451
twist shape parameters	θ_o (deg)	0.204	0.177	0.120
	θ_1 (deg)	-36.82	-25.40	-16.15
	θ_2 (deg)	7.43	11.72	36.30
	θ_3 (deg)	-17.79	-18.85	-20.57
sweep parameters	ε_1	0.0349	0.0704	0.2680
	ε_2	0.0707	0.2680	0.2533

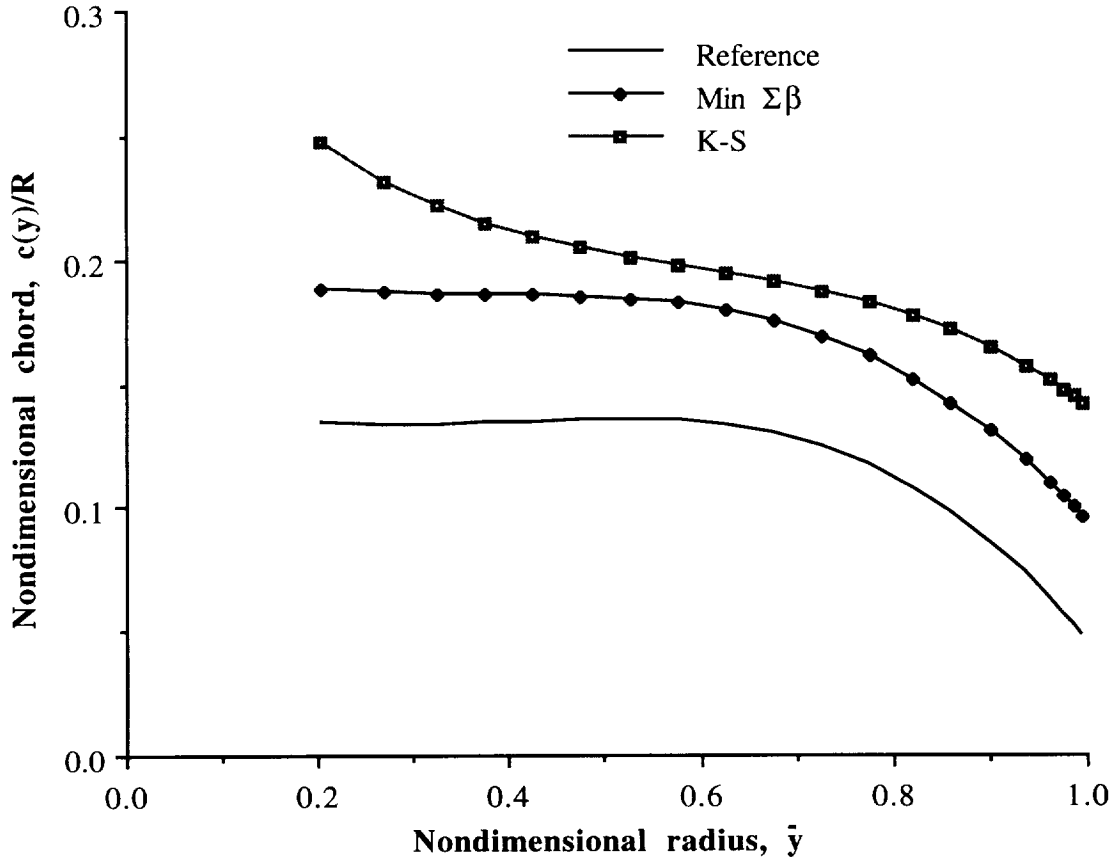

Figure 23 Chord distribution

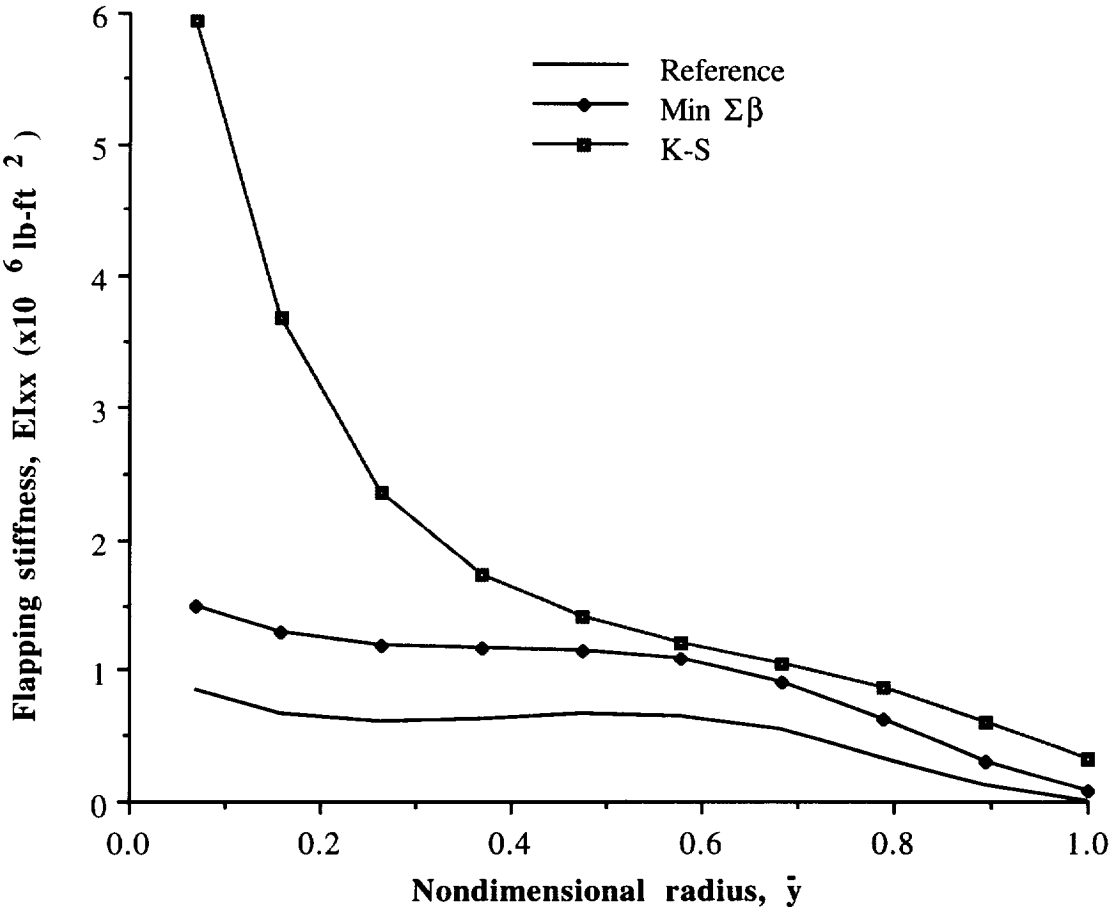

Figure 24 Flapwise bending stiffness distribution

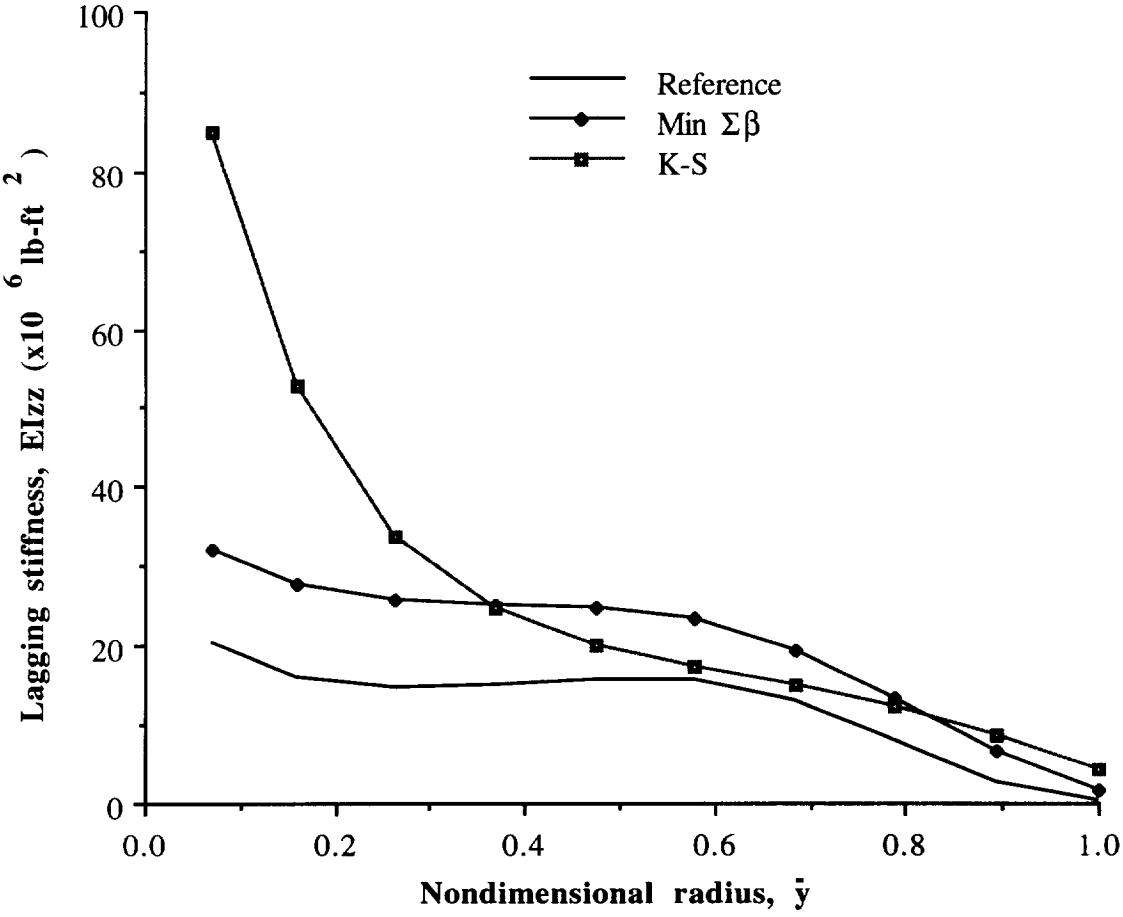

Figure 25 Lead-lag stiffness distribution

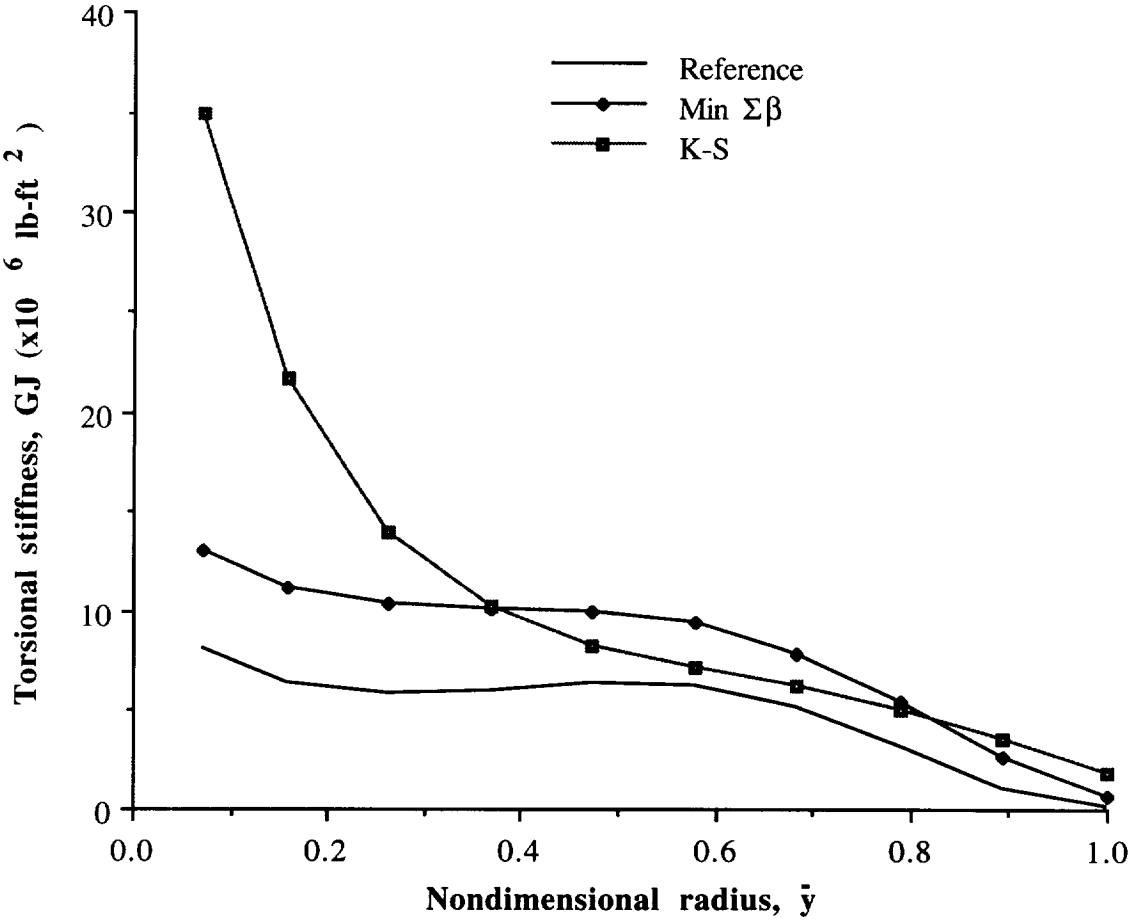

Figure 26 Torsional bending stiffness distribution

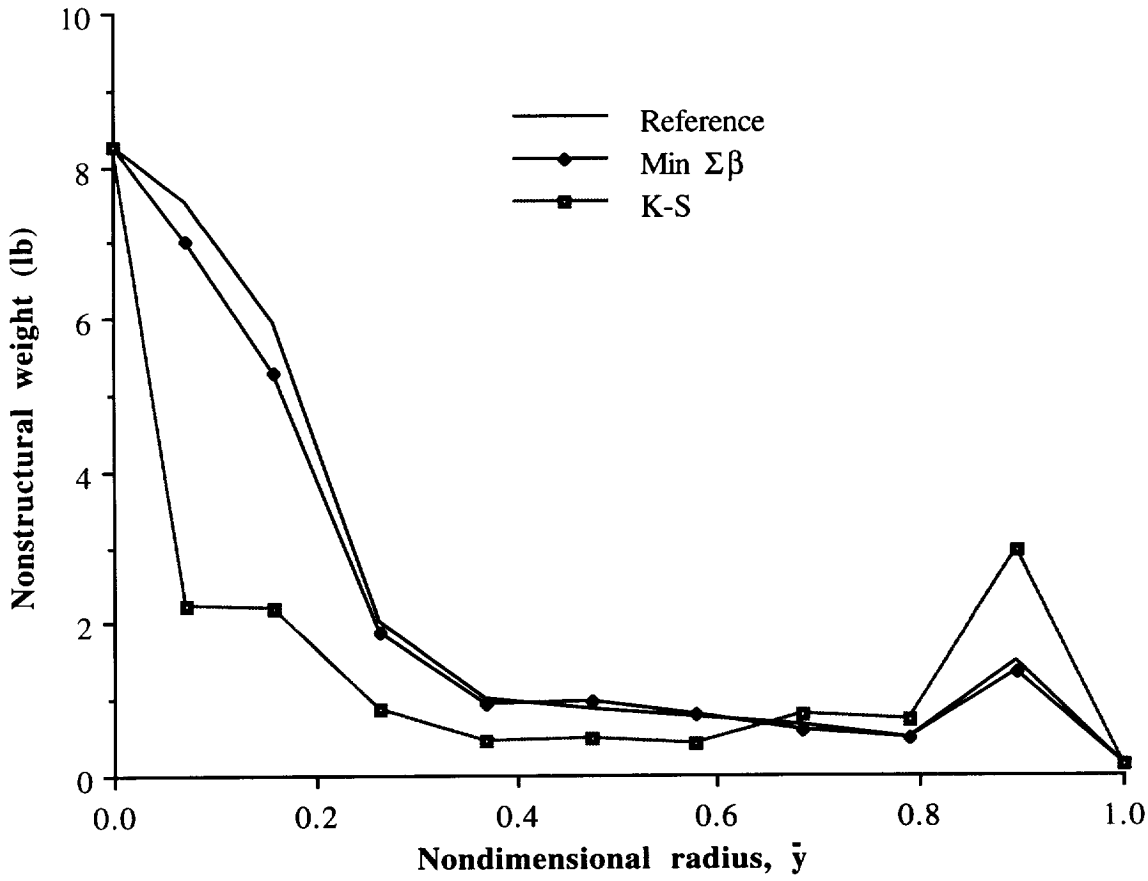

Figure 27 Nonstructural weight distribution

The twist distributions for the optimum rotors and the reference rotor are presented in Fig. 28. The figure indicates that in both the Min $\Sigma\beta$ and the K-S function approaches, the magnitudes of the twist are reduced throughout the blade span from reference to optimum, which is expected at the high forward speed used in cruise. The reductions are more significant in the K-S function case. The distributions are also more nonlinear in nature than the reference blade.

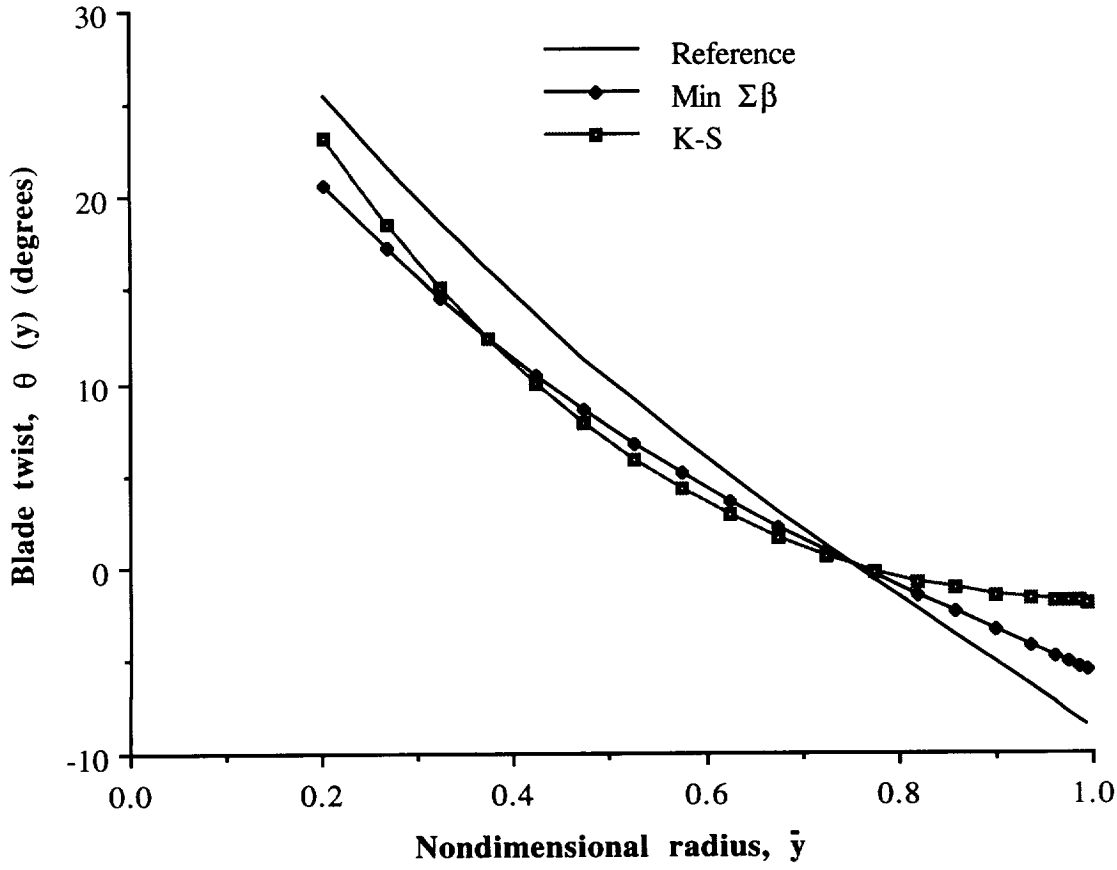

Figure 28 Twist distribution

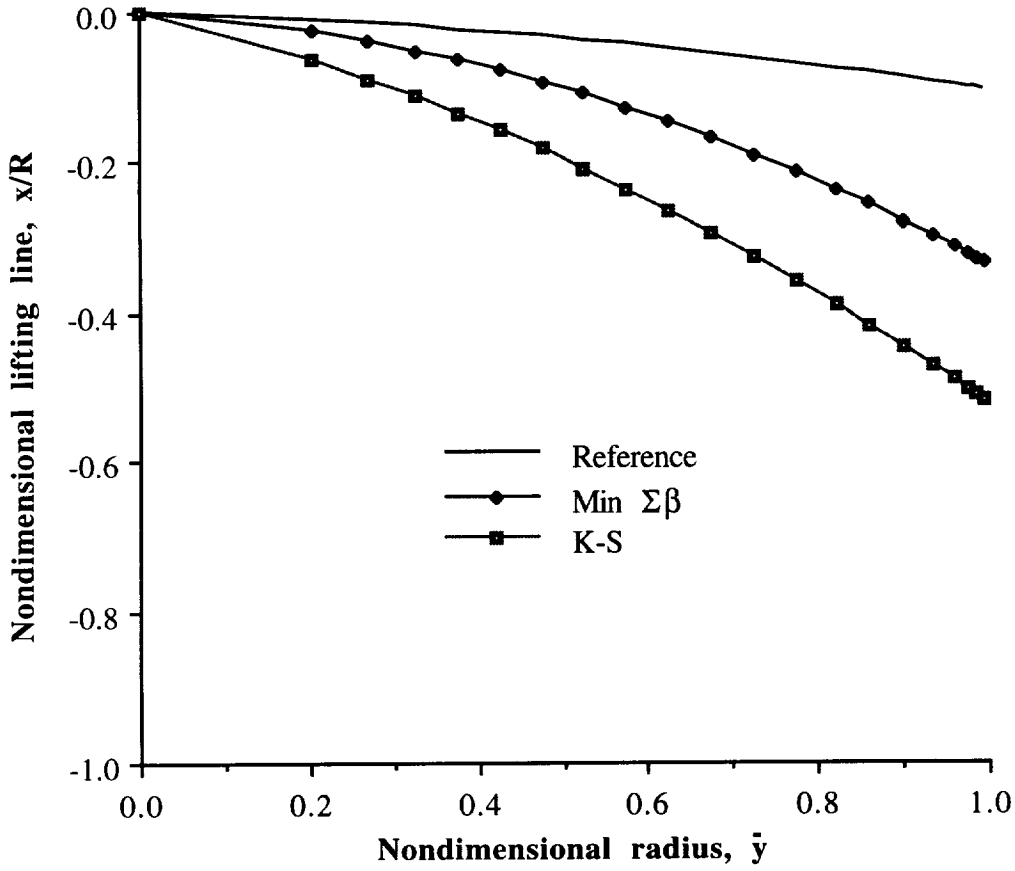

Figure 30 Lifting line distribution

The iteration history of the individual objective functions are presented in Fig. 31. Interestingly, the trends are very similar for the first few cycles in both multiobjective function formulation techniques as the optimizer increases both the individual objective function values in both cases while trying to satisfy the constraints. After that, in the K-S function case, the optimizer increases the hover figure of merit (FOM) while the propulsive efficiency in cruise (η_{ax}) actually decreases. The hover figure of merit then tends to oscillate and the optimizer focuses on increasing η_{ax}. In the Min $\Sigma\beta$ approach, the hover figure of merit starts oscillating quicker than in the K-S function approach (and at a lower value), after which the optimizer steadily increases the propulsive efficiency.

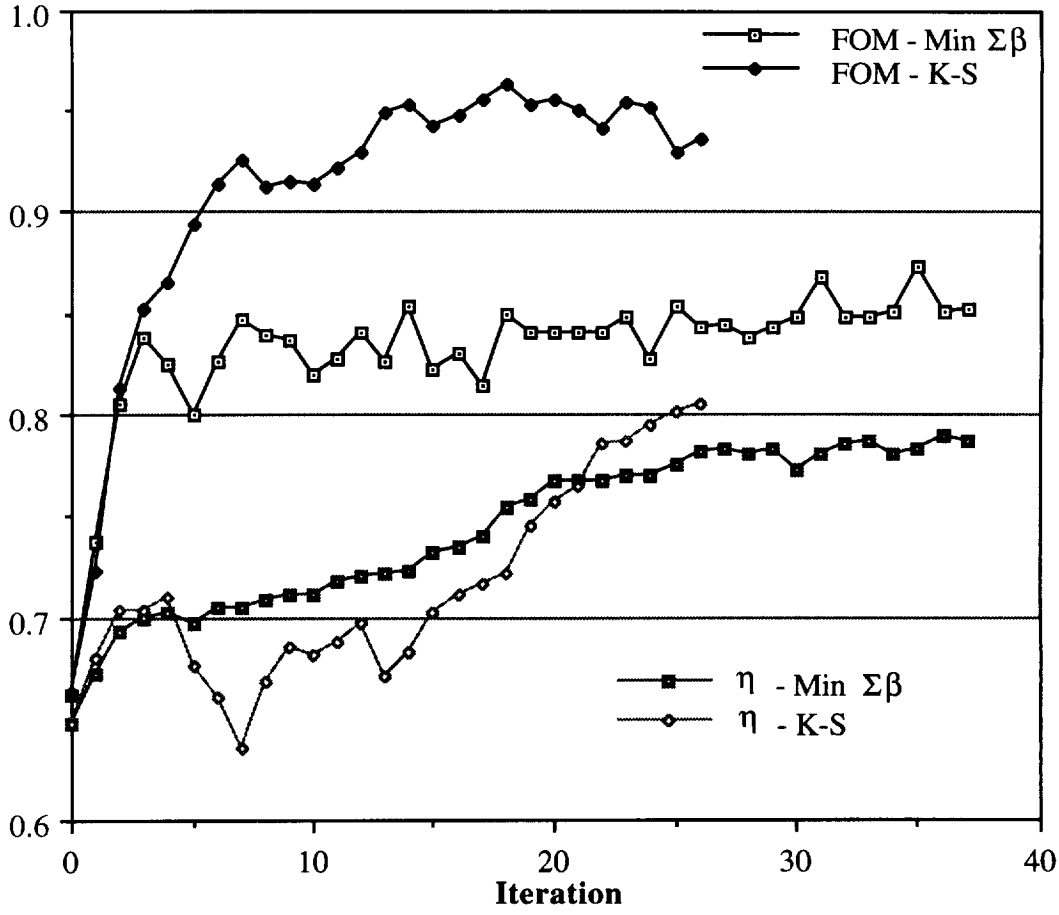

Figure 31 Individual objective function iteration history

The compound objective function iteration history for the Min $\Sigma\beta$ and K-S function approaches is shown in Fig. 32. The figure indicates that the Min $\Sigma\beta$ objective function has smoother convergence to its optimum solution, whereas the objective function in the K-S function case appears to be highly oscillatory in nature. This is expected since the objective function is the Min $\Sigma\beta$ case is strictly linear ($F(\Phi) = \beta_1 + \beta_2$) and the objective function in the K-S function case is different at each iteration, since it is based upon the largest value in the constraint vector for a given iteration (see Eqn. 29). Two different values of the factor (ρ), 250 and 500, are used during the optimization.

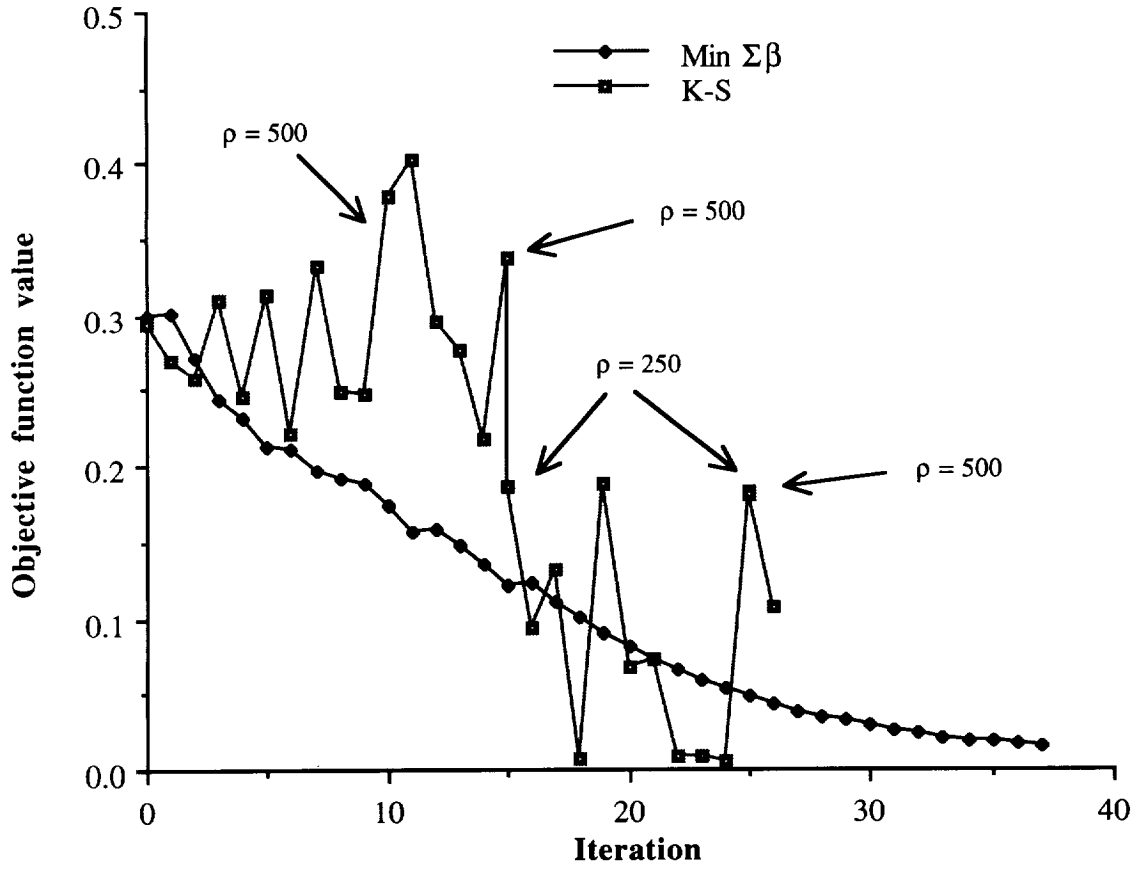

Figure 32 Objective function iteration history

Conclusions

A formal multiobjective optimization procedure was developed to address the complex and conflicting design requirements associated with high-speed prop-rotor design. The objectives were to simultaneously maximize the propulsive efficiency in high-speed cruise and the figure of merit in hover. Constraints were imposed on the aeroelastic stability in axial flight, the first natural frequency in hover and the total blade weight. Both structural and aerodynamic design variables were used. From this problem, the following conclusions were made.

1) Both the high-speed propulsive efficiency and hover figure of merit are substantially increased using the Min $\Sigma\beta$ and the K-S function approaches.
2) The optimum rotor solidity is significantly increased using both multiobjective formulation techniques to satisfy the first natural frequency constraint in hover.
3) Both optimum blades are highly swept and have less total twist than the reference blade.
4) The nonstructural tuning mass distribution differs significantly from the reference values in the K-S function case.

VI. References

1. Ashley, H., "On Making Things the Best - Aeronautical Use of Optimization," *AIAA J. of Aircraft*, 19, No. 1, 1982.

2. Sobieszczanski-Sobieski, J, "Structural Optimization Challenges and Opportunities," Presented at the Int. Conf. on Modern Vehicle Design Analysis, London, England, June 1983.

3. Sobieszczanski-Sobieski, J, editor, "Recent Experiences in Multidisciplinary Analysis and Optimization," NASA CP - 2327, 1984.

4. Magee, J. P., Maisel, M. D. and Davenport, F. J., "The Design and Performance of Propeller/Rotors for VTOL Applications," *Proc.*, 25th Annual AHS Forum, May 1981.

5. Gessow, A. and Myers, G. C., Aerodynamics of the Helicopter, College Park Press, 1985.

6. Reichert, G., "Helicopter Vibration Reduction - A Survey," *Vertica*, Vol. 5, pp. 1-20, 1981.

7. Friedmann, P. P., "Application of Modern Structural Optimization to Vibration Reduction in Rotorcraft," *Vertica*, Vol. 9, No. 4, 1985, pp. 363-373.

8. Taylor, R. B., "Helicopter Vibration Reduction by Rotor Blade Modal Shaping", *Proc.*, 38th Annual Forum of the AHS, May 4-7, 1982, Anaheim, California.

9. Bennett, R. L., "Application of Optimization Methods to Rotor Design Problems," *Vertica*, Vol. 7, 1983.

10. Peters, D. A., Ko, T., Rossow, M. P., "Design of Helicopter Rotor Blades for Desired Placement of Natural Frequencies," *Proc.* of the 39th Annual Forum of the AHS, May 9-11, 1983, St. Louis, Missouri.

11. Friedmann, P.P. and Shantakumaran, P., "Aeroelastic Tailoring of Rotor Blades for Vibration Reduction in Forward Flight," AIAA paper No. 83-0914, *Proc.*, 24th AIAA SDM Conference, Lake Tahoe, NV, Vol. 2, May 1983, pp. 344-359.

12. Hanagud, S., Chattopadhyay, A., Yillikci, Y. K., Schrage, D., and Reichert, G., "Optimum Design of a Helicopter Rotor Blade," Paper No. 12, *Proc.*, 12th European Rotorcraft Forum, September 22-25, 1986, Garmisch-Partenkirchen, West Germany.

13. Pritchard, J. I. and Adelman, H. M. A., "Optimal Placement of Tuning Masses for Vibration Reduction in Helicopter Rotor Blades," *Proc.*, 29th AIAA SDM Conference, Williamsburg, VA, April, 1988.

14. Chattopadhyay, A. and Walsh, J. L., "Minimum Weight Design of Rectangular and Tapered Helicopter Rotor Blades with Frequency Constraints," *Proc.*, 2nd Int. Conference on Rotorcraft Basic Research, February 16-18, 1988, College Park, Maryland. Journal of the AHS, October 1989.

15. Chattopadhyay, A. and Walsh, J. L., "Minimum Weight Design of Rotorcraft Blades with Multiple Frequency and Stress Constraints," *Proc.* AIAA/ASME/ASCE/AHS 29th Structures, Structural Dynamics and Materials Conference, Williamsburg, Virginia, April 18-20, 1988. AIAA Paper No. 88-2337-CP. AIAA Journal, March 1990.

16. Weller, W. H. and Davis, M. W., "Application of Design Optimization Techniques to Rotor Dynamics Problems," *Proc.*, 42nd Annual Forum of the AHS, Washington, D.C., June 2-4, 1986, pp. 27-44.

17. Weller, W. H. and Davis M. W., "Experimental Verification of Helicopter Blade Designs Optimized for Minimum Vibration," *Proc.*, 44th Annual Forum of the AHS, June 16-18, 1988, Washington, D. C.

18. Walsh, J. L., Bingham, G. J. and Riley, M. F., "Optimization Methods Applied to the Aerodynamic Design of Helicopter Rotor Blades," *Journal of the AHS*, Vol. 32(4), Oct. 1987, pp. 39-44.

19. Kumar, S. and Bassett, D., "Rotor Performance Optimization for Future Light Helicopters," *Proc.*, 43rd Annual AHS Forum, St. Louis, MO, May 1987.

20. Nixon, M. W., "Preliminary Structural Design of Composite Main Rotor Blades for Minimum Weight," NASA TP - 2730, July 1987.

21. Celi, R. and Friedmann, P. P., "Efficient Structural Optimization of Rotor Blades with Straight and Swept Tips," *Proc.*, 13th European Rotorcraft Forum, Arles, France, September 1987. Paper No. 3-1.

22. Lim, J., W. and Chopra, I., "Aeroelastic Optimization of a Helicopter Rotor," *Proc.*, 44th Annual Forum of the AHS, June 16-18, 1988, Washington, D. C.

23. Chattopadhyay, A., Walsh, J. L. and Riley, M. F., "Integrated Aerodynamic/Dynamic Optimization of Helicopter Blades," *Proc.*, AIAA/ASME/ASCE/AHS 30th Structures, Structural Dynamics and Materials Conference, Mobile, Alabama, April 3-5, 1989. AIAA Paper No. 89-1269. Special Issue of the *AIAA J. of Aircraft*, January 1991.

24. Chattopadhyay, A. and Chiu, Y. D., "Details of an Enhanced Aerodynamic/Dynamic Optimization Procedure for Helicopter Rotor Blades," NASA CR - 181899

25. He, C. and Peters, D. A. "Optimization of Rotor Blades for Combined Structural, Dynamic, and Aerodynamic Properties," *Proc.*, Third Air Force/NASA Symposium on Recent Advances in Multidisciplinary Analysis and Optimization, San Francisco, CA, Sept. 24-26, 1990.

26. Straub, F., Callahan, C. B. and Culp, J. D., "Rotor Design Optimization Using A Multidisciplinary Approach," Paper No. AIAA 91-0477. Presented at the 29th Aerospace Sciences Meeting, Jan. 7-10, 1991, Reno, Nevada.

27. Chattopadhyay, A. and McCarthy, T. R.., "Multiobjective Design Optimization of Helicopter Rotor Blades with Multidisciplinary Couplings," Optimization of

Structural Systems and Industrial Applications, editors, Hernandez, S. and Brebbia, C.A., pp. 451-462, 1991.

28. Chattopadhyay, A. and McCarthy, T. R.., "Multidisciplinary Optimization Approach for Vibration Reduction in Helicopter Rotor Blades," *Computers and Mathematics with Applications* (in print)

29. Chattopadhyay, Aditi and McCarthy, Thomas R., "A Sensitivity Study In Integrated Optimum Design of Helicopter Rotor Blades," *proc.* 4th Annual AIAA/USAF/NASA/OAI Symposium on Multidisciplinary Analysis and Optimization, Cleveland, Ohio, September 21-23, 1992.

30. Chattopadhyay, Aditi and McCarthy, Thomas R., "Recent Efforts at Multicriteria Design Optimization of Helicopter Rotor Blades," *proc.* NATO/DFG ASI International Conference, "Optimization of Large Structural Systems," Berchtesgaden, Germany, September 23 - Oct. 4, 1991.

31. Chattopadhyay, Aditi and McCarthy, Thomas R., "Optimum Design of Helicopter Rotor Blades with Multidisciplinary Couplings," Paper No. AIAA 92-0214. *proc.* 30th Aerospace Sciences Meeting, January 6-9, 1992, Reno, Nevada.

32. Vanderplaats, G. N., "CONMIN - A Fortran Program for Constrained Function Minimization," User's Manual, NASA TMX-62282, August 1973.

33. Johnson, W., "A Comprehensive Analytical Model of Rotorcraft Aerodynamics and Dynamics," Part II: User's Manual, NASA TM 81183, June 1980.

34. Johnson, W., "A Comprehensive Analytical Model of Rotorcraft Aerodynamics and Dynamics - Johnson Aeronautics Version," Vol. II. User's Manual.

35. Talbot, P., Phillips, J. and Totah, J., "Selected Design Issues of Some High Speed Rotorcraft Concepts," presented at the AIAA/AHS/ASEE Aircraft Design, Sytems and Operations Conference, September 17-19, 1990, Dayton, Ohio.

36. Rutherford, J., O'Rourke, M., Martin, C., Lovenguth, M. and Mitchell, C., "Technology Needs for High Speed Rotorcraft," NASA CR 177578, NAS2 - 13070, April 1991.

37. Wilkerson, J. B., Schneider, J. J. and Bartie, K. M., "Technology Needs for High Speed Rotorcraft (1)," NASA CR 177585, NAS2 - 13041, May 1991.

38. Scott, M. W., "Technology Needs for High Speed Rotorcraft (2)," NASA CR 177590, NAS2 - 13058, August 1991.

39. Detore, J. and Conway, S., "Technology Needs for High Speed Rotorcraft (3)," NASA CR XXXX, NAS2 - 13072, 1991.
177578

40. Lamon, S., "XV-15 Advanced Technology Blade, Ultimate Stress Analysis," Boeing Report Number D210-12345-1, 1985.